A numerical stability investigation of strong ZND detonations for Majda's model

Blake Barker * Kevin Zumbrun[†]
May 29, 2022

Abstract

We carry out a systematic numerical stability analysis of ZND detonations of Majda's model with Arrhenius-type ignition function, a simplified model for reacting flow, as heat release and activation energy are varied. Our purpose is, first, to answer a question of Majda whether oscillatory instabilities can occur for high activation energies as in the full reacting Euler equations, and, second, to test the efficiency of various versions of a numerical eigenvalue-finding scheme suggested by Humpherys and Zumbrun against the standard method of Lee and Stewart. Our results suggest that instabilities do not occur for Majda's model with Arrhenius-type ignition function, nor with a modified Arrhenius-type ignition function suggested by Lyng–Zumbrun, even in the high-activation energy limit. We find that the algorithm of Humpherys–Zumbrun is in the context of Majda's model 100-1,000 times faster than the one described in the classical work of Lee and Stewart and 1-10 times faster than an optimized version of the Lee–Stewart algorithm using an adaptive-mesh ODE solver.

1 Introduction

In this paper, we carry out a systematic numerical stability investigation for detonation solutions of Majda's model with Arrhenius-type ignition function in the high-activation energy limit, at the same time testing and comparing various different techniques for numerical stability analysis. Our results should have application also to the effective design of numerical methods for more complicated detonation models.

Majda's model [M1], a simplified model for reacting compressible gas dynamics, is often used as a testing ground for theory and numerical methods designed for application to the more complicated reacting compressible Euler equations [BMR, M2]. A question posed by Majda in [M2] is whether this simplified model is sufficient to capture the complicated

^{*}Indiana University, Bloomington, IN 47405; bhbarker@indiana.edu: Research of B.B. was partially supported under NSF grant no. DMS-0801745.

[†]Indiana University, Bloomington, IN 47405; kzumbrun@indiana.edu: Research of K.Z. was partially supported under NSF grants no. DMS-0300487 and DMS-0801745.

Hopf bifurcation/pulsating instability phenomena that occur for the full equations in the high-activation energy limit.¹ To explore this theoretical question is one motivation for the present work.

A second motivation comes from the numerics themselves. In their foundational paper [LS] on numerical stability analysis, in which they introduce the standard scheme now in use, Lee and Stewart describe the numerical determination of detonation stability as computationally intensive, and identify the development of more efficient schemes as an important problem in the physical detonation theory.²

We take advantage, therefore, of the simplified context of Majda's model, as a proving ground for various different numerical schemes, in particular testing whether recently-developed techniques from the related problem of stability of viscous shock waves [HuZ2, HLZ, HLyZ, BHZ, Z3] can be imported in a useful way.

Our main object is to test whether an alternative "Evans function-type" scheme proposed by Humpherys–Zumbrun [HuZ1] can outperform the standard scheme of Lee–Stewart, at the same time exploring optimal implementations for both. There is some reason to hope for improvement, since, as pointed out in [HuZ1], the Lee–Stewart shooting method can be reformulated as an adjoint Evans computation carried out in a backward direction, the direction from x=0 toward $x=-\infty$ in which eigenfunctions (normal modes) are required to decay. (See also Section 5.2.) As pointed out in [Br, BrZ, HuZ2, Z3], there is a numerical advantage in shooting, rather, in the direction $x=-\infty$ toward x=0 that eigenfunctions are expected to grow, since error modes then decay exponentially relative to the mode being computed, with the advantage being proportional to the spectral gap between growing and decaying modes of the eigenvalue ODE.

Other novelties of our investigation are the systematic use of adaptive-step mesh both in spatial and frequency variables, the development of higher-order high-frequency asymptotics, the derivation of rigorous if sometimes conservative bounds on the maximum size of unstable eigenvalues, and the introduction of a hybrid and limiting schemes designed for the singular, square-wave limit.

1.1 Results

Our results are, first, that Majda's model does not appear to support instabilities of any kind for Arrhenius or modified Arrhenius ignition function, even in the high-activation energy limit. (For zero activation energy, see the analytical proof of [JY].)

Second, it does appear that the optimum version found for the Humpherys–Zumbrun scheme outperforms the optimum version found for the Lee–Stewart scheme, by a factor of

¹ "In particular, ... there is the possibility of *Hopf bifurcation* to pulsating reacting fronts with an associated exchange of stability..." – problem 1, p. 25, [M2].

² "Finally, we point out that even though our scheme is direct and easy to implement, complete investigation of the various regions of parameter space is computationally intensive. Any equivalent or more efficient numerical method for computation of detonation should be considered a valuable contribution and such approaches are needed to further explore the parameter regimes of instability." – closing paragraph, p. 130, [LS].

1-10 depending on frequency, and on the average perhaps 2-4. However, this difference is dwarfed by the (scheme independent) one obtained by using an adaptive-step ODE solver in the x-evolution, which yields improvement over the fixed-mesh solver originally used in [LS] by a factor of 100-1000. Likewise, in our implementation, the difference between the implicit z-coordinatization of [Er2, LS], in which the profile is explicitly solvable as a function of z, and the x-coordinatization in which the problem presents itself, is improvement by a uniform factor of 6 (apparently due to the cost of evaluating the profile; see Remark 4.2).

The message is that the choice of numerical scheme requires a bit of care. For, with the wrong choices, performance can degrade by a total factor of as much as 2400-24000! With all the right choices, on the other hand, the computation is for reasonable values of activation energy quite numerically well-conditioned, at least in the simplified context of Majda's model, with computation times on the order of that seen for a scalar or 2×2 viscous conservation law, of a few seconds for an entire stability computation for a given set of model parameters.

In the high-activation energy limit, as for any singular limit, the computational performance degrades. In such cases, we find it necessary to factor out as much growth/decay of the solution as we possibly can, with less effective schemes not even converging for reasonable precisions and computation times.

1.2 Discussion and open problems

As observed by Majda [M2], the Majda model may be derived from the full reacting compressible Euler equations via weakly nonlinear geometric optics in certain limiting regimes. However, as noted in [Z1], these can be seen to lie in the small heat-release/small-activation energy region for which detonations are known to be stable [Z4]. Thus, there is no physical reason to expect that parallels should extend to the high-activation energy limit and associated pulsating instability phenomena.

Nonetheless, the structural analogy between the equations persists, and so the observed results of universal stability are somewhat striking. It would be interesting to pursue further the difference between the two models, both at formal and rigorous levels. In particular, a very interesting open problem is the analytic verification of stability for general \mathcal{E} , as done for $\mathcal{E} = 0$ in [JY].

A novelty here as regards detonation literature is the derivation of rigorous bounds on the size of unstable eigenvalues. However, these in some cases degrade rapidly in the singular, high-activation energy limit, blowing up as $e^{O(\mathcal{E})}$ as $\mathcal{E} \to \infty$.³ Indeed, our convergence studies show these bounds to be much too conservative, suggesting a sharp bound rather of $O(\mathcal{E})$. The application of semiclassical limit/turning point techniques to obtain better bounds would be a very interesting technical question; see Remark 6.6. Another very interesting open problem would be to carry out a complete stability analysis in the limit as $\mathcal{E} \to \infty$, a problem intermediate to the analysis of general \mathcal{E} . This together with the

³ In some interesting cases, including the square-wave limit, they do not; see Remark 6.7.

numerical studies carried out here for bounded \mathcal{E} , would resolve the question of general \mathcal{E} by a combined numerical and analytical approach, similarly as was done for viscous shock waves in [HLZ, HLyZ, BHZ, BLZ],

We have carried out here a systematic confirmation/examination in a simple context of a number of aspects of numerical detonation stability analysis, which we hope will serve as a useful reference for further developments. In particular, a very interesting direction for future investigation is to determine whether the gains in efficiency observed for Majda's model carry over to the full reacting compressible Euler equations.

2 Preliminaries

2.1 Equations and assumptions

Consider the inviscid Majda model

(2.1)
$$u_t + \left(\frac{u^2}{2}\right)_x = qk\phi(u)z,$$
$$z_t = -k\phi(u)z,$$

 $u, z, \phi, q, k \in \mathbb{R}^1, q \geq 0, k > 0$, with Arrhenius type ignition function

(2.2)
$$\phi(u) = \begin{cases} Ce^{-\mathcal{E}/T(u)} & T > 0, \\ 0 & T \le 0. \end{cases}$$

Here T(u) is a relation approximating the temperature/velocity relation for a full ZND profile. We consider here the simple cases T(u) = u as proposed by Majda [BMR, M1, M2] and $T(u) = 1 - (1 - 1.5)^2$, a downward quadratic relation qualitatively similar to that for the full ZND equations as proposed by Lyng–Zumbrun [LyZ2].

A strong detonation wave of (2.1) is a traveling-wave solution

(2.3)
$$(u,z)(x,t) = (\overline{u},\overline{z})(x-st), \quad \lim_{\xi \to \pm \infty} (\overline{u},\overline{z})(\xi) = (u_{\pm},z_{\pm})$$

in the weak, or distributional, sense, smooth except at a single shock discontinuity, without loss of generality at x = 0, where u jumps from $u_* = \bar{u}(0^-)$ to $\bar{u}(0^+)$ as x crosses zero from left to right, with $z_- = 0$, $z_+ = 1$, $u_- > u_i > u_+$, and

$$(2.4) u_{-} > s > u_{+},$$

where u_i , defined as the minimum value of u for which $T(u_i) = 0$, is the ignition temperature. That is, a strong detonation wave consists of a shock advancing to the right into a quiescent (i.e., nonreacting) constant state with reactant mass fraction z = 1, raising u above ignition level u_i , followed by a smooth "reaction tail" in which combustion (reaction) occurs, in which z decays exponentially to value $z_- = 0$ and u to $1 \le u_- < u_*$ as $x \to -\infty$ [Er1, M1, LyZ1, LyZ2, JLW, Z1, Z2].

2.2 Parametrization

By the invariances of (2.1), we may take without loss of generality $u_* = 2$, $u_+ = 0$, s = k = 1, and C > 0 arbitrary, leaving only the parameters $q \ge 0$ and $\mathcal{E} \ge 0$. From (2.4) and the assumption that (\bar{u}, \bar{z}) converges as $x \to \pm \infty$, we find [JY, Z1] that

(2.5)
$$(\bar{u}, \bar{z})(x) \equiv (u_+, z_+) = (0, 1) \text{ for } x > 0$$

and also (see (2.7) below) $u_{-} = 1 + \sqrt{1 - 2q}$, so that

$$(2.6) 1 \le u_{-} \le 2, \quad 0 \le q \le \frac{1}{2}.$$

with activation energy \mathcal{E} varying in the infinite range $0 \leq \mathcal{E} < +\infty$.

2.3 Profiles

The ZND profile equations may be written, adding q times the second equation to the first, as $-s(\overline{u}+q\overline{z})'+\left(\frac{\overline{u}^2}{2}\right)'=0$ and $-s\overline{z}'+k\phi(\overline{u})\overline{z}=0$. Integrating the first equation from $-\infty$ to x and solving the resulting quadratic, we obtain (see [JY, Z1] for details)

(2.7)
$$\overline{u}(x) = 1 + \sqrt{1 - 2q(1 - \overline{z}(x))}.$$

We then obtain \bar{z} by solving the ODE

(2.8)
$$z' = k\phi(u(z))z, \quad z(0) = 1.$$

In the simplest case $\mathcal{E} = 0$, we have the explicit solution $\bar{z} = e^{kx}$.

2.4 Square-wave structure and the high-activation energy limit

In the high-activation energy limit $\mathcal{E} \to 0$, the profile ODE becomes singular, with variation in \bar{z} concentrated near the value u_{max} for which the "temperature function" T(u)is maximized. For the Arrhenius case T(u) = u, this means concentration near the value $u_{max} = \bar{u}(0^{-}) = 2$ at the right endpoint x = 0 of the profile, and results in a sharpened reaction spike near that point; see Figure 2. Here, following the standard normalization of [Er2, LS], we have chosen C in (2.2) so that $\bar{z}(-2) = 1/2$, that is, the half-reaction occurs at a specified spatial point x = -2. For the modified Arrhenius case $T(u) = 1 - (u - 1.5)^2$, rather, $\phi(2) \to 0$ exponentially in \mathcal{E} , and so the profile takes on a characteristic "squarewave" shape similarly as for the full reacting Euler equations, consisting of a long flat tail from $x = -\infty$ to an intermediate point x_0 for which $\bar{u}(x_0) = u_{max} = 1.5$, a rapid change in the vicinity of x_0 , and a second long flat region from $x = x_0$ to x = 0; see Figure 1. Here, we have chosen a bit less carefully the normalization $C = e^{21\mathcal{E}/40}$ in order to keep in frame the value of x at which z = 1/2. (Recall that change in C amounts to rescaling in x, so is not essential to our analysis.) For the full equations, square-wave structure and the high-activation energy limit are associated with Hopf bifurcation and transition to instability [Er1, Er2, LS].

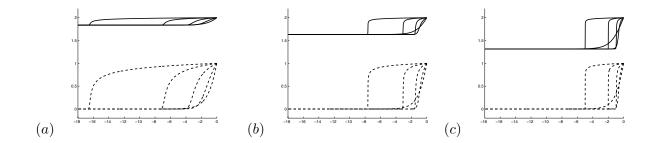


Figure 1: Profile plots for fixed q value and $\mathcal{E}=1,\ 10,\ 20,\ 30,\ 40$. We use a solid line for \bar{u} and a dashed line for \bar{z} plotted against x. Here $\phi(u)=Ce^{-\mathcal{E}/T(u)},\ T(u)=1-(1.5-u)^2,$ and $C=10^{21\mathcal{E}/40}.$ In Figure (a), q=0.15; (b), q=0.3; (c), q=0.45.

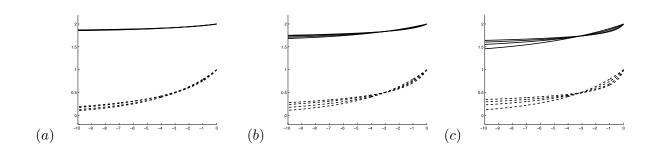


Figure 2: Profile plots for fixed q value and $\mathcal{E}=1,\ 10,\ 20,\ 30$. We use a solid line for \bar{u} and a dashed line for \bar{z} plotted against x. Here $\phi(u)=Ce^{-\mathcal{E}/u}$, where C is chosen so that $\bar{z}(-2)=1/2$. In Figure (a), q=0.15; (b), q=0.3; (c), q=0.45.

3 Linearized stability and the Evans–Lopatinski determinant

We now briefly review the linearized stability theory of [Er1, JLW, Z1, HuZ1]. Shifting to coordinates $\tilde{x} = x - st$ moving with the background Neumann shock, write (2.1) as $W_t + F(W)_x = R(W)$, where

$$(3.1) \hspace{1cm} W := \begin{pmatrix} u \\ z \end{pmatrix}, \quad F := \begin{pmatrix} u^2/2 - su \\ -sz \end{pmatrix}, \quad R := \begin{pmatrix} qkz\phi(u) \\ -kz\phi(u) \end{pmatrix}.$$

To investigate solutions in the vicinity of a discontinuous detonation profile, we postulate existence of a single shock discontinuity at location X(t), and reduce to a fixed-boundary problem by the change of variables $x \to x - X(t)$. In these coordinates, the problem becomes $W_t + (F(W) - X'(t)W)_x = R(W)$, $x \neq 0$, with jump condition X'(t)[W] - [F(W)] = 0, $[h(x,t)] := h(0^+,t) - h(0^-,t)$ as usual denoting jump across the discontinuity at x = 0.

3.1 Linearization/reduction to homogeneous form

In moving coordinates, \bar{W}^0 is a standing detonation, hence $(\bar{W}^0, \bar{X}) = (\bar{W}^0, 0)$ is a steady solution of the nonlinear equations. Linearizing about $(\bar{W}^0, 0)$, we obtain the *linearized* equations $(W_t - X'(t)(\bar{W}^0)'(x)) + (AW)_x = EW$, with jump condition $X'(t)[\bar{W}^0] - [AW] = 0$ at x = 0, where $A := (\partial/\partial W)F$, $E := (\partial/\partial W)R$.

Reversing the original transformation to linear order, following [JLW], by the change of variables $W \to W - X(t)(\bar{W}^0)'(x)$, and noting that x-differentiation of the steady profile equation $F(\bar{W}^0)_x = R(\bar{W}^0)$ gives $(A(\bar{W}^0)(\bar{W}^0)'(x))_x = E(\bar{W}^0)(\bar{W}^0)'(x)$, we obtain modified, homogeneous interior equations $W_t + (AW)_x = EW$ together with a modified jump condition accounting for front dynamics of $X'(t)[\bar{W}^0] - [A(W + X(t)(\bar{W}^0)')] = 0$.

3.2 Evans–Lopatinski determinant

Seeking normal mode solutions $W(x,t) = e^{\lambda t}W(x)$, $X(t) = e^{\lambda t}X$, W bounded, of the linearized homogeneous equations, we are led to the generalized eigenvalue equations $(AW)' = (-\lambda I + E)W$ for $x \neq 0$, and $X(\lambda[\bar{W}^0] - [A(\bar{W}^0)']) - [AW] = 0$, where "I" denotes d/dx, or, setting Z := AW, to

$$(3.2) Z' = GZ, \quad x \neq 0,$$

(3.3)
$$X(\lambda[\bar{W}^0] - [A(\bar{W}^0)']) - [Z] = 0,$$

with

$$(3.4) A = \begin{pmatrix} \overline{u} - 1 & 0 \\ 0 & -1 \end{pmatrix}, E = \begin{pmatrix} qkd\varphi(\overline{u})\overline{z} & qk\varphi(\overline{u}) \\ -kd\varphi(\overline{u})\overline{z} & -k\varphi(\overline{u}) \end{pmatrix},$$

and

(3.5)
$$G = (E - \lambda I)A^{-1} = \begin{pmatrix} \frac{qk \, d\phi(\bar{u})\bar{z} - \lambda}{\bar{u} - 1} & -qk\phi(\bar{u}) \\ \frac{-k \, d\phi(\bar{u})\bar{z}}{\bar{u} - 1} & k\phi(\bar{u}) + \lambda \end{pmatrix}.$$

The Lopatinski determinant is then defined as

(3.6)
$$D_{ZND}(\lambda) := \det(Z^{-}(\lambda, 0), \lambda[\overline{W}] + R(0^{-}))|_{x=0},$$

where $Z^{-}(\lambda, \xi)$ is a bounded exponentially decaying solution of (3.2), analytic in λ and tangent as $\xi \to -\infty$ to the subspace of exponentially decaying solutions of the limiting, constant-coefficient equations $Z' = G_{-}Z$, and

$$R(0^-) = \left(\begin{array}{c} qk\varphi(\overline{u}) \\ -k\varphi(\overline{u}) \end{array} \right), \quad [\bar{W}] = \left(\begin{array}{c} -2 \\ 0 \end{array} \right).$$

More precisely, $Z^- \sim e^{\mu_- x} V_-(\lambda)$, where μ_- is the positive real part eigenvalue of G_- and V_- is an associated eigenvector chosen analytically in λ [Br, HuZ2, Z3]. Evidently, there exists a normal mode solution with frequency λ , $\Re \lambda \geq 0$, if and only if $D_{ZND}(\lambda) = 0$.

4 Numerical approximation

To estimate D_{ZND} numerically, we approximate Z^- at a large but finite negative value x = -M with the value $Z^-(-M) = e^{-\mu_- M} V_-$, and solve from -M to 0 using a standard adaptive-step Runga–Kutta scheme. The vector $V_-(\lambda)$ is evolved analytically by solution of Kato's ODE $\partial_{\lambda}V = P'(\lambda)V$, where $P(\lambda)$ is the eigenprojection associated with μ_- ; see [BrZ, Z2, HuZ2, Z3]. Numerical convergence and efficiency of general schemes of this type are discussed in [Br, HuZ2, Z3].

Remark 4.1. As discussed in [HuZ1, Z3], the single most important factor for efficiency of such computations is to use an adaptive-step rather than fixed-step ODE solver since traveling front and boundary-layer solutions inherently involve multiple scales. As seen here, failure to use adaptive steps can reduce efficiency by two or more orders of magnitude.

Detection of roots. Zeros of the Evans–Lopatinski determinant can be found through individual λ -evaluations by Newton's or other root-finding/following methods as in [LS]. Alternatively, as in [Er2, BrZ, HuZ2, Z4], they can be detected by a Nyquist diagram, or winding-number, computation, mapping a large semicircle S contained in the positive real part half-plane $\Re \lambda \geq 0$ via D_{ZND} and taking the winding number to determine the number of zeros lying within S. We follow the latter approach here. We discretize S by adaptive λ -steps, taking care that the relative change in $D_{ZND}(\lambda_j)$ is ≤ 0.2 for each step, thus ensuring an accurate winding number count [Br, BrZ].

z-coordinatization and renormalization. For purposes of numerical approximation, is advantageous to use the coordinatization of Erpenbeck, Lee–Stewart, and others, by z instead of x. This means replacing Z' = GZ by

$$\dot{Z} = \check{G}Z,$$

where denotes d/dz and

(4.2)
$$\check{G}(z) := \frac{G}{\bar{z}'} = \frac{G}{k\phi(u(z))},$$

then integrating from z=0 to z=1 instead of from $x=-\infty$ to x=0. In practice, we integrate from $z=e^{-k\phi(-\infty)M}$ to z=1, where x=-M is our usual starting point in x-coordinatized version, and initialize Z^- as usual as $e^{-\mu M}V_-$. This avoids the need to solve the \bar{z} equation $\bar{z}'=k\phi(\bar{u})\bar{z}$ numerically.

A further (standard; see [Br, HuZ2]) improvement is to renormalize $Z = e^{\int_0^x \mu Y}$, dividing out expected growth/decay, converting $Y' = (G - \mu I)Y$ to $\dot{Y} = HY$, where

(4.3)
$$H(z) := \frac{G - \mu I}{\overline{z}'} = \frac{G - \mu I}{k\phi(u(z))}.$$

Here, μ can be either μ_- or (better if computable analytically) the eigenvalue $\mu(x)$ of G(x).

Remark 4.2. For an adaptive-step ODE solver, we found no mathematical difference between x- and z- coordinates, as both required the same number of mesh points/functional evaluations for a given x (resp z) integration. However, in practice, the change to z-coordinates gave an improvement of 6 times or more in speed due to the cost of the interpolation step used to evaluate the numerically pre-computed profile at the variable points needed for an adaptive step ODE. This could be improved somewhat by the use of a more efficient interpolation scheme; however, z-coordinates are always preferable for an adaptive-step ODE solver. As discussed in [Z3, HuZ1], renormalization typically improves speed for a single λ -evaluation by a factor of 2 or more. This is magnified in the high-activation energy limit, for which growth/decay rates become extreme, and the unrenormalized computation often cannot even be carried out, leaving machine scale and returning NaN errors. For winding number computations, it is still more important to divide out expected growth/decay, which otherwise introduces additional winding, decreasing the λ stepsize and greatly increasing computational cost.

Reduction by λ . By translation-invariance, D_{ZND} has always a root at $\lambda = 0$. Likewise, there is an extra factor λ as $\lambda \to \infty$ induced by the form of factor $(\lambda[\bar{W}^0] + R)$ in the defining determinant beyond what is induced by growth/decay of the ODE solution Z^- ; see also the more detailed discussion of Section 6. For both these reasons, it is advantageous in performing winding-number computations to work with a reduced Evans-Lopatinski determinant $D_{ZND}(\lambda)/\lambda$, effectively removing a single zero, hence one circuit about the origin, and thereby greatly reducing the number of λ -points required for the computation (typically by factor 4 or so); see Figure 3. All winding number computations are done, therefore, with respect to the reduced determinant, throughout the paper.

⁴Additional experiments, not recorded here.

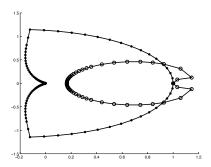


Figure 3: For $\mathcal{E}=10,\ q=0.3,\ C=10^{E/2+E/40}$, and R=4, which we get from the high-frequency convergence study, it takes 2.7524 seconds and 127 mesh points to obtain 0.2 tolerance in the λ contour for the unreduced Evans–Lopatinski determinant D_{ZND} . If we divide by λ , it takes 0.6858 seconds and 28 mesh points. Open circles correspond to the reduced Evans function for which we divide by λ .

5 Alternative formulations

5.1 The adjoint Evans-Lopatinski determinant

We may define an alternative stability function (see [HuZ2, CJLW, Z4]) as

(5.1)
$$\tilde{D}_{ZND}(\lambda) = \langle \tilde{Z}, (\lambda [\bar{W}^0] + R) \rangle|_{x=0},$$

where \tilde{Z} denotes the unique (up to scalar multiplier) decaying solution of

(5.2)
$$\tilde{Z}' = -G^* \tilde{Z}, \quad x \le 0, \qquad -G^* = \begin{pmatrix} \frac{-qk \, d\phi(\bar{u})\bar{z} + \lambda^*}{\bar{u} - 1} & \frac{k \, d\phi(\bar{u})\bar{z}}{\bar{u} - 1} \\ qk\phi(\bar{u}) & -k\phi(\bar{u}) - \lambda^* \end{pmatrix}.$$

 D_{ZND} and \tilde{D}_{ZND} differ by a nonvanishing analytic factor β , by duality relations $\tilde{Z} = \frac{Z^{\perp}}{W}$ and $\det(v, w) = v^{\perp} \cdot w$, where $W = ce^{\int_0^x \operatorname{Trace}(G)}$ is an appropriately normalized Wronskian of (3.2) and $D_{ZND} = \beta \tilde{D}_{ZND}$ with $\beta = W$.

Remark 5.1. The method of reduction to homogeneous form [JLW] is equivalent to solving the inhomogeneous equation

(5.3)
$$\hat{Z}' = G\hat{Z} + \lambda X \bar{W}'(x)$$

by linear superposition, using the fact that a particular solution is given by $W_p = X\bar{W}'(x)$, hence $\hat{W} = W^- + X\bar{W}'(x)$, or $\hat{Z} = Z^- + XA\bar{W}'(x) = Z^- - XR(x)$, and substituting into the jump relation $\lambda X[\bar{W}^0] + [\hat{Z}] = 0$.

As discussed further in [HuZ1], (5.2) may be viewed as a streamlined version of the original method of Erpenbeck [Er2]; we shall refer to this scheme as the *homogeneous Erpenbeck* method. When renormalized by $\tilde{\mu}_{-}$ (resp. $\tilde{\mu}(x)$), we will refer to it as the *adjoint* μ (resp. *adjoint* $\mu(x)$) method.

5.2 The method of Lee and Stewart

The method of Lee and Stewart consists, rather, of solving the inhomogeneous equation (5.3) with X = 1 from x = 0 initialized with $\hat{Z}(0) := \lambda[\bar{W}]$. They then take the inner product of \tilde{V}^- against Z(-M), with M chosen sufficiently large.⁵ By duality, this can be seen to be exactly

(5.4)
$$D_{LS}(\lambda) = \frac{\tilde{D}_{ZND}(\lambda)}{e^{-\bar{\mu}_2(-\infty)(\lambda)M}},$$

where $\mu_2(-\infty)$ is the negative eigenvalue of G_- .

Expanding $\bar{W}' = (d\bar{W}/dz)\bar{z}' = (d\bar{W}/dz)k\phi\bar{z}$, we may rewrite (5.3) in z-coordinates as

(5.5)
$$\dot{\hat{Z}} = \frac{G}{k\phi\bar{z}}\hat{Z} + \lambda \begin{pmatrix} d\bar{u}/d\bar{z} \\ 1 \end{pmatrix},$$

where $d\bar{u}/d\bar{z}$ is determined from the profile solution (2.7). Equivalently

(5.6)
$$\tilde{D}_{ZND}(\lambda) = e^{-\bar{\mu}_2(-\infty)(\lambda)M} D_{LS}(\lambda) = \langle \tilde{V}^-, \hat{Z}_c(-\infty) \rangle,$$

where

(5.7)
$$\dot{\hat{Z}}_c = \frac{G - \mu_2(-\infty)}{k\phi\bar{z}}\hat{Z}_c + \lambda \begin{pmatrix} d\bar{u}/d\bar{z} \\ 1 \end{pmatrix}.$$

Homogeneous version. The Lee–Stewart method may equally well be implemented via the homogeneous equations Z' = GZ, $Z(0) = \lambda[\bar{W}] + R$. (Here, we are using $Z - \hat{Z} \to 0$ as $x \to -\infty$.) This appears to be slightly faster but essentially equivalent in practice.

5.3 The Polar/Drury method

An alternative to direct renormalization is the polar method (or continuous orthogonalization method of Drury) [HuZ2], which, in z coordinates, appears as

(5.8)
$$\dot{Y} = \frac{(G - YY^*G)Y}{\bar{z}'} = \frac{(G - YY^*G)Y}{k\phi(u(\bar{z}))\bar{z}},$$

where $D_{polar}(\lambda) := \det(Y, \lambda[\bar{W}^0] + R)|_{z=1}$. This differs from D_{ZND} by a nonvanishing continuous factor $r(\lambda)$, so has the same winding number and roots. It has the advantage that $|Y| \equiv 1$, so growth/decay is completely factored out, while good numerical conditioning is maintained so long as there remains at least a neutral spectral gap between μ_- and the other eigenvalue of G_- [Z3], as holds in this case on a neighborhood of $\Re \lambda \geq 0$ (see Section 6). An adjoint version can be computed similarly; we refer to this scheme as the polar adjoint method. The factor $r(\lambda)$ may be computed by integrating $\log r = \frac{Y^*GY - \mu_-}{k\phi(u(\bar{z}))\bar{z}}$ from z=0 to z=1, with r(0)=1, and used to recover D_{ZND} [HuZ2]. We refer to the latter scheme as the polar radial, and the analogous dual as the polar adjoint radial method.

⁵ More precisely, since they work like Erpenbeck in z and not x coordinates, against $Z|_{z=\varepsilon}$, $\varepsilon > 0$ sufficiently small. This is phrased in terms of a progress variable $\lambda := 1 - z$; what they call α is our λ .

5.4 Hybrid and limiting methods

In the high-activation energy limit $\mathcal{E} \to 0$ with modified Arrhenius-type ignition function, \bar{u} approaches the well-known "square-wave" profile familiar from the full ZND equations [FD, Er1], which consists approximately of three constant zones separated by a reaction jump following at some distance the Neumann shock. This singular configuration is difficult for the standard numerical Evans-Lopatinski function to resolve, since the integration passes through an unexpected second, different, constant region for which it is not tuned. Indeed, following the numerical prescription of [Z3], we should for best numerical conditioning rather perform an Evans function type computation integrating from $-\infty$ forward toward the reaction jump and from 0 backwards toward the reaction jump, taking a determinant in between.

This can conveniently be accomplished by a hybrid method intermediate to the adjoint and Lee–Stewart methods, in which we compute from z=0 to z=1/2 by the adjoint method, in some optimized version, and from z=1 to z=1/2 via the Lee–Stewart method, again in optimized version, taking the inner product at z=1/2. By duality, this gives the same result as the adjoint method with same optimized form.⁶ This should be done only when $\phi(2) << \max \phi$, so that such singular square-wave structure occurs. When this is not the case, the adjoint method is expected to be preferred. However, the hybrid method is safe, in that its numerical conditioning should always lie somewhere between that of the adjoint and Lee–Stewart methods, and captures some of the gain of the adjoint method even when square-wave structure does not occur.

Limiting method. When $\phi(2) \ll \max \phi$, and square-wave structure is truly in effect, we may take a limit *before* computing the hybrid determinant and simply project out decaying modes. That is, we may define a projective, limiting, method, in which we substitute for initial data $\lambda[\bar{W}] + R$ the data $P(\lambda)(\lambda[\bar{W}] + R)$, where $P(\lambda)$ is the eigenprojection of $G|_{z=1}$ associated with the negative real part eigenvalue μ_2 . For related analytical results in a similar situation, see [Z5]. We will refer to this version as the *Evans function* method.

6 High frequency asymptotics

Making the change of coordinates $x \to \hat{x} := |\lambda| x$, $\lambda \to \hat{\lambda} := \lambda/|\lambda|$, we convert (5.2) to the approximately diagonal system

(6.1)
$$\dot{\tilde{Z}} = A(\varepsilon \hat{x})\tilde{Z} + \varepsilon B(\varepsilon \hat{x})\tilde{Z},$$

where $|\hat{\lambda}| = 1$, $\Re \hat{\lambda} \ge 0$, $\varepsilon := |\lambda|^{-1}$, denotes $d/d\hat{x}$, and

$$(6.2) A = \begin{pmatrix} \frac{\hat{\lambda}^* - \varepsilon q k \, d\phi(\bar{u})\bar{z}}{\bar{u} - 1} & 0 \\ 0 & -\lambda^* - \varepsilon k \phi(\bar{u}) \end{pmatrix}, B = \begin{pmatrix} 0 & \frac{k \, d\phi(\bar{u})\bar{z}}{\bar{u} - 1} \\ q k \phi(\bar{u}) & 0 \end{pmatrix}.$$

In practice, we solve $Z' = (G - \mu_2(x))Z$, where μ_2 is the negative eigenvalue of G, and the adjoint version $\tilde{Z}' = -(G - \mu_2(x))^* \tilde{Z}$.

Making the further change of coordinates $\tilde{Z} = TY$,

$$T = \begin{pmatrix} 1 & \varepsilon a \\ \varepsilon b & 1 \end{pmatrix}, \qquad T^{-1} = (1 - \varepsilon^2 a b)^{-1} \begin{pmatrix} 1 & -\varepsilon a \\ -\varepsilon b & 1 \end{pmatrix},$$

$$(6.3) a = \frac{k \, d\phi(\bar{u})\bar{z}}{-\bar{u}\hat{\lambda}^* - \varepsilon(k\phi(\bar{u}) + qk \, d\phi(\bar{u})\bar{z})}, b = \frac{qk\phi(\bar{u})(\bar{u} - 1)}{\bar{u}\hat{\lambda}^* + \varepsilon(k\phi(\bar{u}) + qk \, d\phi(\bar{u})\bar{z})},$$

we obtain

(6.4)
$$\dot{Y} = T^{-1}(A + \varepsilon B)TY - T^{-1}\dot{T}Y = A_1Y + \varepsilon^2 B_1Y + \varepsilon^3 B_2Y,$$

where

(6.5)
$$A_1 = \begin{pmatrix} \alpha_1 & 0 \\ 0 & \alpha_2 \end{pmatrix} := \begin{pmatrix} \frac{\hat{\lambda}^* - \varepsilon q k \, d\phi(\bar{u})\bar{z}}{\bar{u} - 1} & 0 \\ 0 & -\lambda^* - \varepsilon k \phi(\bar{u}) \end{pmatrix},$$

$$(6.6)$$

$$B_{1} = \begin{pmatrix} -aqk\phi(\bar{u}) + \frac{bk d\phi(\bar{u})\bar{z}}{\bar{u}-1} - ab(\lambda^{*} + k\phi(\bar{u})) & -a^{2}qk\phi(\bar{u}) + \frac{a_{x}}{1-\varepsilon^{2}ab} \\ \frac{b_{x}}{1-\varepsilon^{2}ab} + \frac{b^{2}k d\phi(\bar{u})\bar{z}}{\bar{u}-1} & aqk\phi(\bar{u}) - \frac{bk d\phi(\bar{u})\bar{z}}{\bar{u}-1} - ab\frac{\hat{\lambda}^{*} - qk d\phi(\bar{u})\bar{z}}{\bar{u}-1} \end{pmatrix},$$

$$B_{2} = \begin{pmatrix} \frac{-ab_{x}}{1-\varepsilon^{2}ab} & 0 \\ 0 & \frac{ba_{x}}{1-\varepsilon^{2}ab} \end{pmatrix}.$$

6.1 Estimation of Z^-

Change now to \hat{y} -coordinates, where $d\hat{x}/d\hat{y} = \phi(\bar{u}(\hat{x}))$, i.e., $d\bar{z}/d\hat{y} = \varepsilon k\bar{z}$, or $\bar{z}(y) = e^{k\varepsilon\hat{y}}$. Defining $Y(\hat{y}) = e^{\int_0^{\hat{y}} \alpha_1(\hat{z})d\hat{z}}V(\hat{y})$, and simplifying, we obtain as usual the Duhamel representation:

(6.7)
$$V(\hat{y}) = \mathcal{T}V(y) := V_{-} + \int_{-\infty}^{\hat{y}} e^{\int_{\hat{z}}^{\hat{y}} (\hat{A}_{1} - \hat{\alpha}_{1}I)(\hat{s})d\hat{s}} (\varepsilon^{2}\hat{B}_{1} + \varepsilon^{3}\hat{B}_{2})V(\hat{z})d\hat{z},$$

where $\hat{A} = A/\phi$, $\hat{\alpha}_j = \alpha_j/\phi$, $\hat{B}_j = B_j/\phi$, and $|\hat{B}_1(\hat{y})| \leq C_1 e^{-k\varepsilon|\hat{y}|}$, $|\hat{B}_2(\hat{y})| \leq C_2 e^{-k\varepsilon|\hat{y}|}$ for some $C_j > 0$, and $V_- = V_-(\hat{\lambda}) = c(\hat{\lambda})(1,0)^T$ is the asymptotic limit at $\hat{x} \to -\infty$, $c \neq 0$. Here, by the Mean Value Theorem, $C_j \leq \sup |d\hat{B}_j/dz|$. From $\alpha_2 - \alpha_1 = \frac{-\bar{u}\hat{\lambda}^* - \varepsilon k\phi(\bar{u}) + \varepsilon qk \, d\phi(\bar{u})\bar{z})}{\bar{u}-1}$, we have by positivity of $\varepsilon k\phi(u_-)$, $\Re \hat{\lambda} \bar{u}$, and $\bar{u} - 1$, the bound

$$(6.8) |e^{\int_{\hat{z}}^{\hat{z}} (\hat{A}_1 - \hat{\alpha}_1)(\hat{z}) d\hat{z}}| < e^{\int_{\hat{z}}^{\hat{y}} \Re(\hat{\alpha}_2 - \hat{\alpha}_1)(\hat{z}) d\hat{z}} < e^{\gamma \int_{\hat{z}}^{\hat{y}} \frac{d\bar{z}}{d\hat{z}} d\hat{z}} < e^{\gamma \bar{z}(\hat{y})} < e^{\gamma},$$

(6.9)
$$\gamma := q \sup_{x} \left(\frac{(d\phi/\phi)^{\mathcal{P}}}{\bar{u} - 1} \right),$$

where $f^{\mathcal{P}}$ denotes the positive part of f. For $\Re \lambda \geq \max \frac{qkd\phi \bar{z} - k\phi}{\bar{u}}$, we have simply

$$(6.10) |e^{\int_{\hat{z}}^{\hat{z}} (\hat{A}_1 - \hat{\alpha}_1)(\hat{z}) d\hat{z}}| \le e^{\int_{\hat{z}}^{\hat{y}} \Re(\hat{\alpha}_2 - \hat{\alpha}_1)(\hat{z}) d\hat{z}} \le 1.$$

Remark 6.1. For the Arrhenius-type ignition function $\phi(u) = Ce^{\frac{-\mathcal{E}}{u}}$, we have

(6.11)
$$d\phi/\phi = \mathcal{E}/u^2 > 0, \text{ hence } \gamma = q\mathcal{E}/u_-^2 \le q\mathcal{E}.$$

For the modified Arrhenius ignition function $\phi(u) = Ce^{-\frac{\mathcal{E}}{T(u)}}$, where $T(u) = 1 - (u - 1.5)^2$, we have

(6.12)
$$d\phi/\phi = -2(\mathcal{E}/T^2)(u - 1.5), \text{ hence } \gamma \le (4/3)q\mathcal{E} \text{ for } q \ge .375$$

and

(6.13)
$$\gamma \equiv 0 \text{ for } q \leq .375, \text{ in which case } \bar{u} \geq u_- \geq 1.5 \text{ and } d\phi/\phi \leq 0.$$

A sufficient condition for $\Re \lambda \geq \max \frac{qkd\phi \bar{z} - k\phi}{\bar{u}}$, is

$$\Re \lambda \ge k \gamma \max \phi \sim k \mathcal{E} \max \phi.$$

Lemma 6.2. For $\varepsilon \leq \frac{k}{2e^{\gamma}(C_1+\varepsilon C_2)}$ or $\varepsilon \leq \frac{k}{2(C_1+\varepsilon C_2)}$ and $\Re \lambda \geq \max \frac{qkd\phi \bar{z}-k\phi}{\bar{u}}$, \mathcal{T} is a contraction on $L^{\infty}(-\infty,0]$, and $\tilde{Z}^-|_{\hat{x}=0}$ is proportional to $(1,\omega_2)^T$, where $\omega_2 := \frac{\varepsilon b(0)+\omega}{1+\varepsilon a(0)\omega}$ and $|\omega| \leq \frac{\varepsilon e^{\gamma}}{k}(C_1+\varepsilon C_2)$.

Proof. From (6.7) and the stated bounds, the Lipshitz norm of \mathcal{T} is bounded by

$$\int_{-\infty}^{\hat{y}} e^{\gamma} \frac{\varepsilon^{2}(C_{1} + \varepsilon C_{2})}{\phi(\hat{z})} e^{-k\varepsilon|\hat{z}|} d\hat{z} \leq \varepsilon e^{\gamma}(C_{1} + \varepsilon C_{2}) \int_{-\infty}^{\hat{y}} e^{-k\varepsilon|\hat{z}|} d\hat{z}$$

$$\leq \varepsilon e^{\gamma}(C_{1} + \varepsilon C_{2}) \int_{-\infty}^{\hat{y}} e^{-k\varepsilon|\hat{z}|} d\hat{z}$$

$$\leq \frac{\varepsilon e^{\gamma}}{k} (C_{1} + \varepsilon C_{2}) e^{-k|\hat{x}|},$$

hence it is contractive for $\frac{\varepsilon e^{\gamma}}{k}(C_1 + \varepsilon C_2) \leq 1/2$, or $\varepsilon \leq \frac{k}{2e^{\gamma}(C_1 + \varepsilon C_2)}$, with relative error at $\hat{x} = 0$ from the diagonal solution (i.e., with ε set to zero) given by $\frac{\varepsilon e^{\gamma}}{k}(C_1 + \varepsilon C_2)$.

That is, Y(0) is proportional to $(1,\omega)^T$, with $|\omega| \leq \frac{\varepsilon e^{\gamma}}{k} (C_1 + \varepsilon C_2)$. Transforming back by $\tilde{Z}^- = TY$, with $T = \begin{pmatrix} 1 & \varepsilon a \\ \varepsilon b & 1 \end{pmatrix}$, we thus find that

$$\tilde{Z}^-|_{\hat{x}=0} = T = \begin{pmatrix} 1 & \varepsilon a \\ \varepsilon b & 1 \end{pmatrix} \begin{pmatrix} 1 \\ \omega \end{pmatrix} = \begin{pmatrix} 1 + \varepsilon a \omega \\ \varepsilon b + \omega \end{pmatrix}$$

is proportional to $(1, \omega_2)^T$, where $\omega_2 := \frac{\varepsilon b(0) + \omega}{1 + \varepsilon a(0)\omega}$.

Remark 6.3. Lemma 6.2 may be recognized as a variable-coefficient analog of the gap lemma of [GZ], and a quantitative version of the abstract Lemma A.1 established for the full ZND system in [Z4]. Though we did not state it, the argument implies also that \tilde{Z}^- converges exponentially in relative error as $x \to -\infty$ to the solution of the diagonal system $\tilde{Z}' = A_1 \tilde{Z}$, A_1 as in (6.5). A similar argument applies for the related polar method [HuZ2].

Corollary 6.4. $D_{ZND}(\lambda) \neq 0$ for $0 \leq \Re \lambda$ and

$$|\lambda| \ge \max\{\frac{2e^{\gamma}}{k}(C_1 + \varepsilon C_2), \frac{k\phi(2)}{2}(q + |\omega_2|)\}, \qquad \omega_2 := \frac{\varepsilon b(0) + \omega}{1 + \varepsilon a(0)\omega}.$$

or

$$\Re \lambda \geq \max \frac{qkd\phi \bar{z} - k\phi}{\bar{u}} \quad and \quad |\lambda| \geq \frac{k\phi(2)}{2}(q + |\omega_2|), \qquad \omega_2 := \frac{\varepsilon b(0) + \omega}{1 + \varepsilon a(0)\omega}.$$

Proof. Computing $\lambda[\bar{W}] + R(\bar{W}(0^-)) = (-2\lambda + qk\phi(2), -k\phi(2))^T$, we have that $D_{ZND}(\lambda)$ is proportional by a nonvanishing analytic factor to

$$\langle \tilde{Z}^{-}(\lambda,0), (-2\lambda + qk\phi(2), -k\phi(2))^{T} \rangle|_{x=0} = (1,\omega_{2})^{T} \cdot (-2\lambda + qk\phi(2), -k\phi(2))^{T},$$

and thus to $(1, \omega_2)^T \cdot (-2\hat{\lambda} + \varepsilon q k \phi(2), -\varepsilon k \phi(2))^T = -2\hat{\lambda} + \varepsilon k \phi(2)(q - \omega_2)$, which is nonvanishing provided $\varepsilon k \phi(2)(q + |\omega_2|) \le 2$, or $\varepsilon \le \frac{2}{k\phi(2)(q + |\omega_2|)}$.

Remark 6.5. When $|\lambda| \geq \frac{2e^{\gamma}}{k}(C_1 + \varepsilon C_2)$, $|\omega| \leq 1$, so that $|\omega_2|$ is roughly 1 as well, and $\frac{k\phi(2)}{2}(q + |\omega_2|) \lesssim \frac{3k\phi(2)}{4}$.

Remark 6.6. Corollary 6.4 is efficient for λ near the real axis. However, for the Arrhenius-type ignition function T(u) = u it can be quite inefficient away from the real axis, where it does not make sufficient use of spectral separation of modes as opposed to spectral gap, hence requires the unusable bound $|\lambda| \geq e^{\gamma} \sim e^{\mathcal{E}}$ as $\mathcal{E} \to \infty$. To obtain practical (guaranteed) bounds by use of more modern turning-point theory is an important direction for future investigation.⁷

Remark 6.7. For the modified Arrhenius ignition function (quadratic version), our estimates are efficient for $q \leq .375$, where $\gamma = 0$: in particular for the "difficult" case q = 0.3 we have much investigated; see Remark 6.1.

Remark 6.8. For q bounded from 1/2, k = 1 and $\mathcal{E} \equiv 0$, C = 1, we have $\gamma = 0$, $a \equiv 0$, and b, b_x roughly 1, giving $C_2 \sim C_1 \sim 1$. Thus, $\varepsilon \lesssim 1$ is sufficient in this case for contraction, or $|\lambda| \gtrsim 1$. Our bounds blow up in the CJ limit $q \to 1/2$, for which $(\bar{u}-1) \to 0$ as $x \to -\infty$. (However, note that $b \to 0$ as $q \to q_{cj}$, partly compensating for badness of this limit.) This case would be interesting for further investigation.

6.2 Limiting behavior

By arguments like those of Section 6.1 and especially Remark 6.3, we find that

$$Z^{-}(0) \sim \begin{pmatrix} e^{\int_{-\infty}^{0} (\beta_{2}(\hat{y}) - \beta_{2}(-\infty)d\hat{y}} \\ 0 \end{pmatrix} = \begin{pmatrix} e^{k \int_{-\infty}^{0} (\phi(\bar{u}(y)) - \phi(\bar{u}(-\infty)))dy} \\ 0 \end{pmatrix}$$

as $\varepsilon \to 0$, where $\beta_2 := -\alpha_2^* = \lambda + \varepsilon k \phi(\bar{u})$, α_2 as in (6.5), yielding the following asymptotic behavior.

⁷ For the Arrhenius-type ignition function, actual instabilities for $\mathcal{E} \to \infty$ are expected to appear (if indeed they do) only in the region $|\lambda| \leq \max qkd\phi\bar{z} \sim E\max\phi$ where spectral separation $|\alpha_1 - \alpha_2| >> 1$ fails.

Proposition 6.9. For $\Re \lambda \geq 0$,

$$(6.16) D_{ZND}(\lambda) = C\lambda(1 + O(\lambda^{-1})), \tilde{D}_{ZND}(\lambda) = C_1\lambda e^{C_2\lambda}(1 + O(\lambda^{-1})).$$

as $|\lambda| \to \infty$, where $C := 2e^{k \int_{-\infty}^{0} (\phi(\bar{u}(y)) - \phi(\bar{u}(-\infty)))dy}$, C_1 , and C_2 are real constants.

Remark 6.10. Higher order approximants $D_{ZND}(\lambda) = e^{C_1\lambda + C_0 + C_{-1}\lambda^{-1}}\lambda(1 + O(\lambda^{-2}))$, etc., may be obtained by further diagonalizations as discussed in [Z4, MaZ3].

In particular, $D \sim 2\lambda$ for $\mathcal{E} = 0$. These relations can be used to determine a maximum radius through a convergence study, which, as pointed out in [HLZ, HLyZ], in practice typically gives better bounds than those obtained by rigorous tracking/conjugation bounds.

7 Numerical experiments

7.1 Initialization at $-\infty$

In our numerical experiments we compute the Lopatinski determinant given in (3.6). Following [Z2, Z3], we use the ODE

$$(7.1) S' = P'S$$

of Kato to explicitly compute an analytically varying initializing eigenvector \tilde{V}^- for the Evans function, where ' denotes $d/d\lambda$, $S(\lambda)$ is the desired eigenvector of $G_{-\infty}$, and $P(\lambda)$ is the associated eigenprojection. Preserving analyticity in this manner, we are able to employ the argument principle thus determining the number of zeros of the Evans function inside a contour by computing the winding number. At $x = -\infty$,

(7.2)
$$G_{-\infty} = \begin{pmatrix} a\lambda & b \\ 0 & c+\lambda \end{pmatrix},$$

where $a = \frac{-1}{\bar{u}-1} = \frac{-1}{\sqrt{1-2q}}$, $b = -qk\phi_-$, and $c = k\phi_-$. Then right and left eigenvectors of $G_{-\infty}$ corresponding to the eigenvalue $c + \lambda$, which satisfies $\Re(c + \lambda) > 0$ for $\Re\lambda > 0$, are respectively $r_+ = \begin{pmatrix} \frac{-b}{(a-1)\lambda-c} \\ 1 \end{pmatrix}$, $l_+ = \begin{pmatrix} 0 & 1 \end{pmatrix}$. We then have the projection $P = \frac{r_+l_+}{l_+r_+}$, and

it's derivative (with respect to λ) P', $P = \begin{pmatrix} 0 & \frac{-b}{(a-1)\lambda - c} \\ 0 & 1 \end{pmatrix}$, $P' = \begin{pmatrix} 0 & \frac{b(a-1)}{((a-1)\lambda - c)^2} \\ 0 & 0 \end{pmatrix}$. Solving the ODE S' = P'S, we find that

(7.3)
$$S(\lambda) = \alpha_2 \begin{pmatrix} \frac{-b}{(a-1)\lambda - c} \\ 1 \end{pmatrix} + \alpha_1 \begin{pmatrix} 1 \\ 0 \end{pmatrix},$$

where we take $\alpha_1 = 0$ and $\alpha_2 = 1$. The corresponding initializing vector for the adjoint method is $\tilde{V}_- = \begin{pmatrix} 1 \\ \frac{b}{(a-1)\lambda^* - c} \end{pmatrix}$.

7.2 Computation of Z^- /evaluation of D

Following the general approach of [HuZ2, HLZ, BHZ], the ODE calculations for individual λ are carried out using MATLAB's ode45 routine, which is the adaptive 4th-order Runge-Kutta-Fehlberg method (RKF45). This method is known to have excellent accuracy with automatic error control. Our standard error tolerance setting is AbsTol = 1e-6 and RelTol = 1e-8 unless otherwise mentioned, and the value of approximate minus spatial infinity -M is determined experimentally by the requirement that the absolute error

$$|(\bar{u}, \bar{z})(-M) - (u, z)_{-\infty}| \le TOL$$

be within a prescribed tolerance, say $TOL = 10^{-3}$, where (\bar{u}, \bar{z}) and $(u, z)_{-\infty}$ are the profile and limiting endstates of Section 2.3. In the rescaled z coordinates where we do not even need the profile to compute, we perform a convergence study of the Evans–Lopatinski determinant for $\lambda = 2i$ to determine numerical infinity, requiring relative error between output be less than 10^{-3} between successive computations for numerical infinity decreasing as negative powers of 2. For a theoretical convergence analysis in the simple case considered here, see [Br]; for a more general treatment, see [Z3]. For the results of a numerical convergence study, see Fig. 4 below.

Fixed-mesh Lee-Stewart implementation. For comparison purpose, we carry out also experiments using a fixed-mesh grid as prescribed in [LS], taking $\varepsilon = 1/N$, and using a uniform mesh for $z \in [0,1]$ of mesh points $z_j = j/N$, then choosing N large enough to get a prescribed level of convergence, as determined by numerical convergence study.

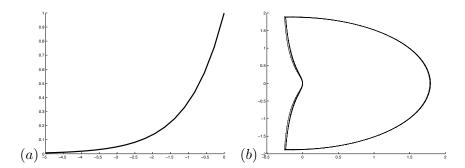


Figure 4: a) Convergence of the profile. b) Convergence of Evans approximations (regular method with $\mu(x)$ scaled out) on a contour with R=1, for $\phi\equiv 1,\ q=0.3,\ k=1$ and approximate spatial infinity $M=0.9,\ 0.5,\ 10^{-1},\ 10^{-2},\ 10^{-3}$. Run times were respectively 1.08, 0.40, 0.76, 1.06, 1.33 seconds.

7.3 Verification: comparison with exact solution

For comparison, we test our code against an exact solution found in [JY] for $\phi \equiv 1$ of

(7.4)
$$D_{ZND}(\lambda) = \left(2\lambda + (2 - q - qk\Psi)\right) \left(\frac{\lambda}{k + \lambda}\right),$$

where

$$(7.5) \quad \Psi := \int_{-\infty}^{0} e^{-\int_{y}^{0} \frac{\lambda}{\sqrt{1 - 2q(1 - e^{ks})}} ds} \frac{e^{(k + \lambda)y}}{\sqrt{1 - 2q(1 - e^{ky})}} dy, \qquad P(\xi) := \frac{\lambda}{\sqrt{1 - 2q(1 - e^{k\xi})}}.$$

This formula results from a choice of Z^- asymptotic to $e^{(\lambda+k)x}(*,1)^T$ as $x\to=\infty$ in agreement with (7.3), hence should agree with the results of our code. As seen in Figure 5, the agreement of code with exact formulat is excellent.

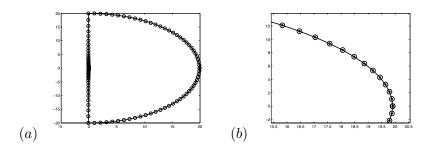


Figure 5: Comparison in the complex plane to the exact solution of [JY] evaluated on a semicircle of radius R=10. a) full size. b) zoom top right. Open circles correspond to the exact solution and the line with closed points to the $\mu(x)$ method. Here $\mathcal{E}=0$ so that $\phi\equiv 1,\,k=1,$ and q=0.3.

7.4 Winding number computations

To check stability, finally, we determine the number of roots within a semicircle $S = \partial B(0,R) \cap \{\Re \lambda \geq 0\}$ of large radius R by computing the winding number of the image curve D(S) as S is traversed counterclockwise, which, by the Principle of the Argument, is equal to the number of roots within. We compute this winding number by varying values of λ around S along 20 points of the contour, with mesh size taken quadratic in modulus to concentrate sample points near the origin where angles change more quickly, and summing the resulting changes in $\arg(D(\lambda))$, using $\Im \log D(\lambda) = \arg D(\lambda) (\bmod 2\pi)$, available in MATLAB by direct function calls. As a check on winding number accuracy, we test a posteriori that the change in argument of D for each step is less than 0.2, and add mesh points, as necessary to achieve this. Recall, by Rouché's Theorem, that accuracy is preserved so long as the argument varies by less than π along each mesh interval.

Computations were carried out within the MATLAB-based STABLAB code developed by J. Humpherys with help of the authors. Using MATLAB's parallel computing toolbox on an 8-core Power Macintosh workstation, we were able to achieve a speedup of over 600%, similarly as in the previous numerical studies [BHZ, BLZ, BLeZ].

Determination of R. The radius R is chosen so large that there exist no unstable roots outside B(0,R), ensuring that the roots found by our winding number computation are the only possible ones on the nonstable half-plane $\Re \lambda \geq 0$. This could be done analytically as

described in Section 6 (and carried out, for example, in [HLyZ]). Here, following instead [BLeZ, BHZ], we use the asymptotics described in Proposition 6.9 Remark 6.10, to match the reduced Lopatinski determinant $D(\lambda)/\lambda$ to a first-order or higher-order approximant $e^{C\lambda}$ or $e^{C_1\lambda+C_0+C_{-1}\lambda^{-1}}$, a carrying out a convergence study to determine when $D(\lambda)/\lambda$ has sufficiently converged.

This was accomplished by, first, requiring that the relative error between $D(\lambda)/\lambda$ and a best-fit value of $Ce^{C_1/\lambda+C_2/\lambda^2}$ be less than or equal to 0.2, and, second, that doubling the radius results in reduction of the error by a factor of approximately two, in accordance with the linear error dependence predicted by analytical theory.

Typical convergence studies are illustrated in Figure 6 and Tables 1 and 2. A comparison of the Evans function vs. reduced Evans function is given in Figure 3.

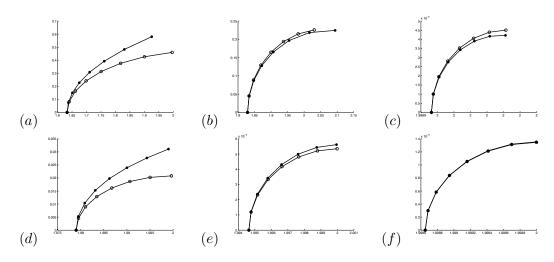


Figure 6: Here we use solid dots to plot the Lopatinski determinant evaluated on a quarter arc, and we use open circles to graph the approximating function, $C_1 \exp(C2/\lambda)$. For the $\mu(x)$ method, we have Figures a-c corresponding respectively to R=2, R=4, and R=2048. For the polar method, we have Figures d-f corresponding respectively to R=4, R=16, R=64. Parameters are $\mathcal{E}=10$, q=0.3, $\phi(u)=Ce^{-\mathcal{E}/T(u)}$, $C=10^{21\mathcal{E}/40}$.

Results. We computed, using the Evans–Lopatinski determinant (our basic algorithm) rescaled by $\mu(x)$, a batch job for the parameter values, $\{\mathcal{E},q\} = \{0.01:0.01:0.49\} \times \{0:0.1:5,\ 5.2:0.2:10,\ 12,\ 15,\ 20,\ 30,\ 40\}$, with the exception of a few numerically challenging parameters $\{E,q\} = \{20\} \times \{0.49\},\ \{30\} \times \{0.48,\ 0.49\},\ \{40\} \times \{0.47,\ 0.48,\ 0.49\},\ \text{with } C = 10^{21\mathcal{E}/40}$, for ignition function $\phi(u) = Ce^{-\mathcal{E}/T(u)}$ where $T(u) = 1 - (u - 1.5)^2$. Computational statistics are given in Table 3. For ignition function $\phi(u) = e^{\mathcal{E}/2}e^{-\mathcal{E}/u}$ we computed the Evans–Lopatinski determinant for $\{\mathcal{E},q\} = \{0:0.1:5,\ 5.2:0.2:10,\ 12,\ 15\} \times \{0.01:0.01:0.37,\ 0.375,\ 0.38:0.01:0.49\} \cup \{20\} \times \{0.01:0.01:0.37,\ 0.375,\ 0.38:0.01:0.47\} \cup \{25\} \times \{0.01:0.20\}$

⁸ For winding number computations, we find that it is important to divide out as much behavior as we can, to avoid excess winding. Dividing by λ is crucial, $C_1eC_2\lambda$ still better. Eventually, there is a break-even point in complexity (and coefficient size of remainder) vs. power of $1/|\lambda|$, here occurring at first order.

Radius	Relative Error	K0	K1	K2
2	0.00387783	0.693873	-0.157136	0.0202546
4	0.000656158	0.693278	-0.152452	0.0110315
8	8.88927e-05	0.693167	-0.150713	0.00427183
16	9.83384e-06	0.69315	-0.150192	0.000241916
32	6.99413e-07	0.693148	-0.15005	-0.00195688
64	1.26154e-07	0.693147	-0.150013	-0.003106
128	5.78215e-08	0.693147	-0.150003	-0.00369357

Table 1: For $\mathcal{E}=10$, q=0.3, $C=e^{\mathcal{E}/2}$, and $\phi(u)=e^{-\mathcal{E}/u}$ we examine the high frequency convergence of the adjoint $\mu(x)$ method with it's best fit with $e^{K0+K1/\lambda+K2/\lambda^2}$.

Radius	Relative Error	K0	K1	K2
2	0.0436173	0.72503	-0.501318	0.0641958
4	0.0294181	0.706568	-0.347815	-0.254427
8	0.0100462	0.696782	-0.190304	-0.88822
16	0.00172202	0.693867	-0.0981737	-1.61602
32	0.000146306	0.693263	-0.0604492	-2.20532
64	6.21728e-05	0.693164	-0.0480715	-2.58952
128	2.54483e-05	0.693149	-0.0444984	-2.81055
256	7.81771e-06	0.693147	-0.0435363	-2.92936
512	2.14819e-06	0.693147	-0.0432867	-2.99093
1024	5.61212e-07	0.693147	-0.0432227	-3.02249

Table 2: For $\mathcal{E} = 10$, q = 0.3, $\phi(u) = Ce^{-\mathcal{E}/T(u)}$, $T(u) = 1 - (1.5 - u)^2$, $C = 10^{21\mathcal{E}/40}$ we examine the high frequency convergence of the adjoint method scaled by $\mu(x)$ to it's best fit with $e^{K0+K1/\lambda+K2/\lambda^2}$.

 $\{0.01:0.01:0.37,\ 0.375,\ 0.38:0.01:0.45\} \cup \{30\} \times \{0.01:0.01:0.37,\ 0.375,\ 0.38:0.01:0.40\}$. Computational statistics are given in Table 4. All computations yielded winding number zero consistent with stability.

q	E=0	E=20	E=30	E=40
0.01	(1e-4,4,10,0.0086,1)	(1e-4,40,10,0.018,1e1)	(1e-4,60,10,0.023,1e1)	(1e-4,80,10,0.026,2e1)
0.1	(1e-4,4,10,0.1,1)	(1e-4,40,21,0.2,3)	(1e-4,60,33,0.19,3)	(1e-4,80,40,0.2,4)
0.2	(1e-4,4,11,0.15,1)	(1e-4,40,39,0.19,3)	(1e-4,60,54,0.2,4)	(1e-4,80,74,0.2,7)
0.3	(1e-4,4,12,0.17,2)	(1e-4,40,49,0.19,3)	(1e-4,60,75,0.19,6)	(1e-4,256,89,0.19,2e1)
0.4	(1e-4,4,17,0.16,2)	(1e-4,40,62,0.2,4)	(1e-4,60,84,0.2,8)	(1e-4,512,107,0.2,4e1)

Table 3: For $\phi = Ce^{-\mathcal{E}/T(u)}$ where $T(u) = 1 - (u - 1.5)^2$ and $C = e^{21\mathcal{E}40}$ we record statistics for our Evans–Lopatinski determinant computations. The data represented are (L,R,error,time) where L is the numerical value of infinity in the spatial z domain, R is the radius of the domain contour, error is the maximum relative error between λ contour output, and time is the time it took to compute.

8 Performance comparisons

In the remainder of the paper, we collect a number of data comparing performance of the various methods.

In Figure 7 we demonstrate agreement between methods that should yield the same output providing a verification of the correctness of our code. This also provides a visual example of which methods require a tighter λ mesh in order to obtain relative error within

	E=0	E=10	E=20	E=30
q = 0.01	(0.1,4,0.004,0.4)	(0.1, 20, 0.0063, 0.8)	(0.1, 40, 0.0075, 1)	(0.1,60,0.0081,2)
q=0.1	(0.1,4,0.045,0.7)	(0.1, 20, 0.073, 2)	(0.1,40,0.088,4)	(0.1,60,0.096,6)
q=0.2	(0.1,4,0.1,1)	(0.1, 20, 0.18, 3)	(0.06,40,0.11,1e+01)	(0.06,60,0.13,2e+01)
q=0.3	(0.1,4,0.18,1)	(0.06, 20, 0.17, 7)	(0.06,40,0.18,2e+01)	(0.03,60,0.18,7e+01)
q=0.4	(0.06,4,0.16,2)	(0.06,20,0.15,1e+01)	(0.03,40,0.17,8e+01)	(0.03,60,0.19,4e+02)

Table 4: For $\phi = e^{\mathcal{E}/2}e^{-\mathcal{E}/u}$ we record statistics for our Evans–Lopatinski determinant computations. Here we use the polar adjoint method with ode solver tolerance set at 10^{-12} . We set the radius of the domain contour to be the max of $2\mathcal{E}$ and the radius obtained by the best curve fit of the Evans–Lopatinski determinant with $e^{E_0+E_1/\lambda+E_2/\lambda^2}$. The data represented are (L,R,error,time) where L is the numerical value of infinity in the spatial z domain, R is the radius of the domain contour, error is the maximum relative error between λ contour output, and time is the time it took to compute.

tolerance.

In Table 6 we demonstrate computational time for the various methods for a fixed λ mesh. In this experiment, we simply set tolerance at $TOL=10^{-12}$ for relative and absolute truncation error in the adaptive RK45 ODE solver and integrated around a fixed radius 10 semicircular contour in the complex λ -plane of the type used in our winding number computations for stability, with a small semicircle of radius 10^{-4} removed around the origin. The time taken to complete this computation gives a rough "average" measure of performance over different λ regimes. However, it is a bit conservative, as it measures truncation and not convergence error, so does not reflect the expected better numerical conditioning of the Humpherys–Zumbrun vs. other schemes. For this reason, we have performed a series of more careful experiments at individual λ -values, specifying convergence rather than truncation error, described below. Note finally that the standard fixed-mesh Lee-Stewart method described in [LS] is not included in the comparisons of Table 6, since, not being adaptive, it does not allow specification of truncation error in this simple way. The important comparison to this scheme is carried out in the convergence error-based study below.

For the convergence error-based study, we evaluate the various methods at the representative values $\lambda=1,\ i,\ 10,\ 10i$ and determine the relative tolerance with which the methods must be solved in order for the output to converge to a specified tolerance. For the methods using an adaptive mesh in z, we specify absolute tolerance to be 10^{-15} and increase relative tolerance by powers of 10 starting at 10^{-1} until consecutive output is less than 10^{-6} in relative error. We use MATLAB's ode45 function which employs the fourth order Runge-Kutta-Fehlberg method. By specifying absolute tolerance to be 10^{-15} , we ensure that relative rather than absolute tolerance determines the mesh setting.⁹

For the fixed z mesh method of Lee and Stewart, we determine a number of mesh points N such that relative error between the fixed mesh inhomogeneous method and the adaptive inhomogeneous method, solved with error tolerance requirements of 10^{-10} , is less than 10^{-6}

⁹ The ode45 algorithm requires that relative tolerance or absolute tolerance be met.

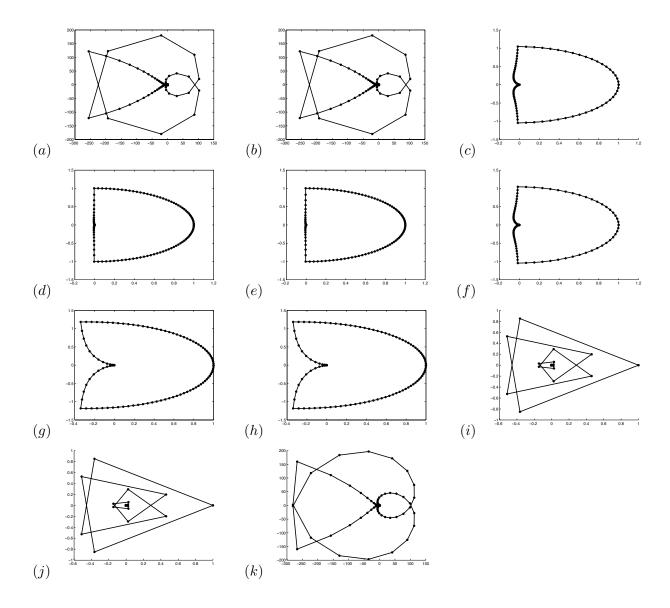


Figure 7: We compare different methods of integration for $\mathcal{E}=10,\ q=0.3,\ \phi(u)=Ce^{-\mathcal{E}/T(u)},\ T(u)=1-(1.5-u)^2,\ \mathrm{and}\ C=10^{21\mathcal{E}/40},\ R=10,\ \mathrm{with}\ 65$ fixed domain mesh points. These comparisons serve as code verification, showing agreement between methods that should give the same output, and contrast the number of points needed by the various methods to obtain output with relative error within tolerance. (a) polar adjoint radial method, (b) adjoint μ method, (c) adjoint $\mu(x)$ method, (d) polar adjoint method, (e) polar method, (f) $\mu(x)$ method, (g) polar radial method, (h) μ method, (i) no μ method, (j) homogeneous Erpenbeck method (k) the homogeneous method of Lee and Stewart

but greater than $9*10^{-7}$. For the fixed z mesh method of Lee and Stewart, the reported tolerance is the relative error between the ODE output of these two methods.

In Tables 7–24 we report the computational statistics for the $\mu(x)$ method, the adjoint $\mu(x)$ method, the hybrid method, the method of Lee and Stewart (adaptive mesh in z), the method of Lee and Stewart (fixed mesh in z), the polar adjoint method, and the polar adjoint radial method, for both ignition functions $\phi(u) = e^{-\mathcal{E}/u}$ and $\phi(u) = e^{-\mathcal{E}/T(u)}$ where $T(u) = 1 - (u - 1.5)^2$. For the first ignition function we record data for $\mathcal{E} = 1$, 10, 20, and q = 0.1, 0.3, 0.47, and for the second ignition function we give statistics for $\mathcal{E} = 0$, 10, 40 and q = 0, 0.3, 0.47. Although not recorded here, we carried out studies for q = 0.2 and q = 0.4 and found the behavior quite similar to that reported.

The outcome, as described in the introduction, is that the Humpherys-Zumbrun algorithm, implemented as $\mu(x)$, polar, or polar radial method, outperforms an optimized, adaptive-mesh, version of the Lee-Stewart algorithm by factor 1-10, and outperforms the actual fixed-mesh version proposed in [LS] by factor 100-1000, even in the high activation energy/square-wave limit. The hybrid method did not perform significantly better in the square-wave limit, and performed significantly worse in other regimes, hence we recommend that this option be discarded. Likewise, the Evans method, valid only when $\phi(2) << \max \phi$, does not seem to perform as well as the basic $\mu(x)$ method (see Table 6), and so does not seem to be worth the trouble of implementation in this special regime. However, this option should perhaps not be discarded without more systematic investigation than was carried out here.

	E=0	E=20	E=30	E=40
q=0.01	(0.0001,4,10,0.0086,1)	(0.0001,40,10,0.018,1e+01)	(0.0001,60,10,0.023,1e+01)	(0.0001,80,10,0.026,2e+01)
q=0.1	(0.0001,4,10,0.1,1)	(0.0001,40,21,0.2,3)	(0.0001,60,33,0.19,3)	(0.0001, 80, 40, 0.2, 4)
q=0.2	(0.0001,4,11,0.15,1)	(0.0001, 40, 39, 0.19, 3)	(0.0001,60,54,0.2,4)	(0.0001,80,74,0.2,7)
q=0.3	(0.0001,4,12,0.17,2)	(0.0001, 40, 49, 0.19, 3)	(0.0001,60,75,0.19,6)	(0.0001,256,89,0.19,2e+01)
q=0.4	(0.0001,4,17,0.16,2)	(0.0001,40,62,0.2,4)	(0.0001,60,84,0.2,8)	(0.0001,512,107,0.2,4e+01)

Table 5: Table of computational statistics, (M,R,points,relative error,time), where -M is the value of numerical negative infinity, R is the radius of the contour used to compute, points is how many points the adaptive solver used to compute the mesh, err is the maximum relative error between two points of the output, and time is how long it took to compute the contour. Here $\phi(u) = Ce^{\mathcal{E}/T(u)}$ where $T(u) = 1 - (1.5 - u)^2$ and C is chosen so that \bar{z} passes through 0.5 at x = -7. Here we are using the $\mu(x)$ method. We take R to be the maximum of $2\mathcal{E}$ and the best root fit with $e^{E_0 + E_1/\lambda + E_2/\lambda^2}$.

method of Lee and Stewart (adaptive mesh in x)	37.0
homogenous method of Lee and Stewart (adaptive mesh in x)	35.8
adjoint $\mu(x)$ method	14.8
hybrid method	27.6
polar adjoint method	13.5
inhomogeneous Erpenbeck method	40.1
polar adjoint radial method	20.8
adjoint μ method	18.2
polar/Drury method	13.5
$\mu(x)$ method	14.5
polar radial method	20.9
μ method	17.9
Evans function method	21.2
homogenous Erpenbeck method	32.4
centered inhomogeneous Erpenbeck method	51.8

Table 6: Computational time comparison on a fixed λ mesh of 55 points with radius 10 and inner radius 10^{-4} for various methods with $E=10,\ q=0.3,\ \phi(u)=e^{-\mathcal{E}/T(u)},\ T(u)=1-(1.5-u)^2,\ C=10^{21\mathcal{E}/40}$ and relative and absolute tolerance is set at 10^{-12} in the ODE solver.

	$\lambda = 1$			$\lambda = i$			$\lambda = 10$			$\lambda = 10i$		
	Tol	Time	pnts	Tol	Time	pnts	Tol	Time	pnts	Tol	Time	pnts
A	-	-	-	-	-	-	-	-	-	-	-	
В	1.0e-2	0.0027	2	1.0e-2	0.0027	2	1.0e-2	0.0026	2	1.0e-2	0.0026	2
C	1.0e-2	0.0077	6	1.0e-2	0.0065	5	1.0e-2	0.014	15	1.0e-2	0.015	14
D	1.0e-2	0.039	37	1.0e-7	0.093	101	1.0e-8	0.88	1098	1.0e-8	1.1	1182
E	6.9e-2	0.025	2	1.1e-7	26	6.55e4	8.5e-7	3.7e + 02	1048580	7.6e-7	420	1048580
F	1.0e-02	0.0027	2	1.0e-02	0.0028	2	1.0e-02	0.0026	2	1.0e-02	0.0026	2
G	1.0e-02	0.0041	3	1.0e-0.2	0.0042	3	1.0e-02	0.0045	3	1.0e-02	0.0043	3

Table 7: Efficiency comparison for several methods: A- the $\mu(x)$ method, B- the adjoint $\mu(x)$ method, C- the hybrid method, D- the method of Lee and Stewart (using an adaptive mesh in z), E- the method of Lee and Stewart using a 4th order fixed mesh Runge Kutta solver, F- the polar adjoint method, and G- the polar adjoint radial method. Here $\mathcal{E}=0$, q=0, $C=10^{21\mathcal{E}/40}$, and $\phi(u)=Ce^{-\mathcal{E}/T(u)}$, $T(u)=1-(u-1.5)^2$.

	$\lambda = 1$			$\lambda = i$			$\lambda = 10$			$\lambda = 10i$		
	Tol	Time	pnts	Tol	Time	Mesh	Tol	Time	Mesh	Tol	Time	Mesh
A	1.0e-02	0.017	12	1.0e-02	0.017	11	1.0e-02	0.067	69	1.0e-02	0.096	93
В	1.0e-04	0.021	16	1.0e-04	0.023	15	1.0e-03	0.07	73	1.0e-05	0.1	104
C	1.0e-02	0.02	14	1.0e-03	0.023	15	1.0e-02	0.075	81	1.0e-04	0.12	121
D	1.0e-08	0.16	191	1.0e-08	0.16	177	1.0e-09	2.1	2603	1.0e-09	2.3	2634
E	5.7e-07	47	131072	6.1e-07	53	131072						
F	1.0e-04	0.021	16	1.0e-05	0.025	19	1.0e-05	0.083	91	1.0e-04	0.099	99
G	1.0e-04	0.0240	24	1.0e-04	0.0271	24	1.0e-05	0.0931	97	1.0e-05	0.1180	109

Table 8: Efficiency comparison for several methods: A- the $\mu(x)$ method, B- the adjoint $\mu(x)$ method, C- the hybrid method, D- the method of Lee and Stewart (using an adaptive mesh in z), E- the method of Lee and Stewart using a 4th order fixed mesh Runge Kutta solver, F- the polar adjoint method, and G- the polar adjoint radial method. Here $\mathcal{E}=0, q=0.3, C=10^{21\mathcal{E}/40}$, and $\phi(u)=Ce^{-\mathcal{E}/T(u)}, T(u)=1-(u-1.5)^2$.

	$\lambda = 1$			$\lambda = i$			$\lambda = 10$			$\lambda = 10i$		
	Tol	Time	pnts	Tol	Time	Mesh	Tol	Time	Mesh	Tol	Time	Mesh
A	1.0e-02	0.022	19	1.0e-02	0.024	18	1.0e-02	0.1	119	1.0e-02	0.17	176
В	1.0e-04	0.029	28	1.0e-04	0.032	28	1.0e-03	0.11	126	1.0e-05	0.2	212
C	1.0e-03	0.028	25	1.0e-04	0.035	30	1.0e-02	0.12	131	1.0e-05	0.23	249
D	1.0e-08	0.31	379	1.0e-08	0.32	367	1.0e-09	4.5	5641	1.0e-09	5	5701
E	4.6e-7	188	524288	4.7e-7	211	524288	-	-	$> 10^{6}$	-	-	
F	1.0e-04	0.027	28	1.0e-05	0.04	38	1.0e-04	0.16	185	1.0e-05	0.2	212
G	1.0e-05	0.0441	45	1.0e-06	0.0705	63	1.0e-06	0.2318	241	1.0e-05	0.2381	220

Table 9: Efficiency comparison for several methods: A- the $\mu(x)$ method, B- the adjoint $\mu(x)$ method, C- the hybrid method, D- the method of Lee and Stewart (using an adaptive mesh in z), E- the method of Lee and Stewart using a 4th order fixed mesh Runge Kutta solver, F- the polar adjoint method, and G- the polar adjoint radial method. Here $\mathcal{E}=0$, q=0.47, $C=10^{21\mathcal{E}/40}$, and $\phi(u)=Ce^{-\mathcal{E}/T(u)}$, $T(u)=1-(u-1.5)^2$.

	$\lambda = 1$			$\lambda = i$			$\lambda = 10$			$\lambda = 10i$		
	Tol	Time	pnts	Tol	Time	Mesh	Tol	Time	Mesh	Tol	Time	Mesh
A	-	-	-	-	-	-	-	-	-	-	-	-
В	1.0e-2	0.0027	2	1.0e-2	0.0028	2	1.0e-2	0.0026	2	1.0e-2	0.0028	2
C	1.0e-2	0.01	10	1.0e-2	0.01	9	1.0e-2	0.021	23	1.0e-2	0.037	39
D	1.0e-8	0.39	485	1.0e-8	0.39	438	1.0e-9	4.9	6134	1.0e-9	6.1	6816
E	2.7e-6	187	524288	2.7e-6	210	524288	-	-	>1e+6	-	-	>1e+6
F	1.0e-02	0.0026	2	1.0e-02	0.0026	2	1.0e-02	0.0025	2	1.0e-02	0.0026	2
G	1.0e-02	0.0040	3	1.0e-02	0.0041	3	1.0e-02	0.0045	3	1.0e-02	0.0050	3

Table 10: Efficiency comparison for several methods: A- the $\mu(x)$ method, B- the adjoint $\mu(x)$ method, C- the hybrid method, D- the method of Lee and Stewart (using an adaptive mesh in z), E- the method of Lee and Stewart using a 4th order fixed mesh Runge Kutta solver, F- the polar adjoint method, and G- the polar adjoint radial method. Here $\mathcal{E}=10$, q=0, $C=10^{21\mathcal{E}/40}$, and $\phi(u)=Ce^{-\mathcal{E}/T(u)}$, $T(u)=1-(u-1.5)^2$.

	$\lambda = 1$			$\lambda = i$			$\lambda = 10$			$\lambda = 10i$		
	Tol	Time	pnts	Tol	Time	Mesh	Tol	Time	Mesh	Tol	Time	Mesh
A	1.0e-6	0.034	29	1.0e-6	0.036	29	1.0e-3	0.035	29	1.0e-4	0.046	38
В	1.0e-5	0.023	19	1.0e-6	0.031	26	1.0e-4	0.042	35	1.0e-4	0.037	32
C	1.0e-6	0.039	38	1.0e-6	0.044	35	1.0e-3	0.036	34	1.0e-4	0.056	52
D	1.0e-6	0.068	68	1.0e-6	0.067	60	1.0e-8	0.38	464	1.0e-8	0.34	381
E	2.6e-7	23	65536	2.6e-7	26	65536	3.6e-7	93	262144	3.8e-7	1.1e+02	262144
F	1.0e-06	0.028	25	1.0e-06	0.033	29	1.0e-03	0.028	26	1.0e-05	0.051	47
G	1.0e-06	0.0422	42	1.0e-06	0.0476	43	1.0e-04	0.0431	43	1.0e-04	0.0451	41

Table 11: Efficiency comparison for several methods: A- the $\mu(x)$ method, B- the adjoint $\mu(x)$ method, C- the hybrid method, D- the method of Lee and Stewart (using an adaptive mesh in z), E- the method of Lee and Stewart using a 4th order fixed mesh Runge Kutta solver, F- the polar adjoint method, and G- the polar adjoint radial method. Here $\mathcal{E}=10$, q=0.3, $C=10^{21\mathcal{E}/40}$, and $\phi(u)=Ce^{-\mathcal{E}/T(u)}$, $T(u)=1-(u-1.5)^2$.

	$\lambda = 1$			$\lambda = i$			$\lambda = 10$			$\lambda = 10i$		
	Tol	Time	pnts	Tol	Time	Mesh	Tol	Time	Mesh	Tol	Time	Mesh
A	1.0e-5	0.032	31	1.0e-6	0.043	40	1.0e-4	0.056	57	1.0e-4	0.068	63
В	1.0e-6	0.04	42	1.0e-7	0.058	58	1.0e-4	0.052	54	1.0e-5	0.083	82
C	1.0e-5	0.036	37	1.0e-6	0.047	46	1.0e-4	0.056	63	1.0e-4	0.071	71
D	1.0e-6	0.074	85	1.0e-7	0.086	94	1.0e-8	0.72	895	1.0e-8	0.79	890
E	6.5e-7	12	32768	1.2e-7	26	65536	7.9e-7	370	$\approx 10^6$	6.9e-7	420	$\approx 10^6$
F	1.0e-06	0.04	39	1.0e-07	0.06	61	1.0e-04	0.053	59	1.0e-05	0.079	82
G	1.0e-07	0.0673	69	1.0e-07	0.0809	74	1.0e-05	0.0825	84	1.0e-05	0.0977	90

Table 12: Efficiency comparison for several methods: A- the $\mu(x)$ method, B- the adjoint $\mu(x)$ method, C- the hybrid method, D- the method of Lee and Stewart (using an adaptive mesh in z), E- the method of Lee and Stewart using a 4th order fixed mesh Runge Kutta solver, F- the polar adjoint method, and G- the polar adjoint radial method. Here $\mathcal{E}=10$, q=0.47, $C=10^{21\mathcal{E}/40}$, and $\phi(u)=Ce^{-\mathcal{E}/T(u)}$, $T(u)=1-(u-1.5)^2$.

	$\lambda = 1$			$\lambda = i$			$\lambda = 10$			$\lambda = 10i$		
	Tol	Time	pnts	Tol	Time	Mesh	Tol	Time	Mesh	Tol	Time	Mesh
A	-	-	-	-	-	-	-	-	-	-	-	-
В	1.0e-02	0.0027	2	1.0e-02	0.0028	2	1.0e-02	0.0027	2	1.0e-02	0.0027	2
C	1.0e-02	0.062	70	1.0e-02	0.14	149	1.0e-02	0.54	617	1.0e-02	1.4	1494
F	1.0e-02	0.0037	2	1.0e-02	0.0027	2	1.0e-02	0.0025	2	1.0e-02	0.0026	2
G	1.0e-02	0.0045	3	1.0e-02	0.0059	3	1.0e-02	0.0061	3	1.0e-02	0.0044	3

Table 13: Efficiency comparison for several methods: A- the $\mu(x)$ method, B- the adjoint $\mu(x)$ method, C- the hybrid method, D- the method of Lee and Stewart (using an adaptive mesh in z), E- the method of Lee and Stewart using a 4th order fixed mesh Runge Kutta solver, F- the polar adjoint method, and G- the polar adjoint radial method. Here $\mathcal{E}=40$, q=0, $C=10^{21\mathcal{E}/40}$, and $\phi(u)=Ce^{-\mathcal{E}/T(u)}$, $T(u)=1-(u-1.5)^2$.

	$\lambda = 1$			$\lambda = i$			$\lambda = 10$			$\lambda = 10i$		
	Tol	Time	pnts	Tol	Time	Mesh	Tol	Time	Mesh	Tol	Time	Mesh
A	1.0e-07	0.096	103	1.0e-07	0.12	112	1.0e-08	0.38	450	1.0e-07	0.37	394
В	1.0e-08	0.18	203	1.0e-07	0.13	134	1.0e-08	0.42	503	1.0e-07	0.64	687
C	1.0e-07	0.1	117	1.0e-07	0.14	145	1.0e-08	0.4	487	1.0e-07	0.79	877
D	1.0e-08	0.2	246	1.0e-07	0.13	143	1.0e-08	0.84	1068	1.0e-08	0.93	1063
E	2.17e-06	5.9	16384	2.06e-06	6.6	16384	4.36e-07	12	32768	3.79e-07	13	32768
F	1.0e-03	0.023	21	1.0e-07	0.12	118	1.0e-03	0.062	67	1.0e-07	0.64	687
G	1.0e-07	0.1338	137	1.0e-07	0.1720	158	1.0e-07	0.3172	334	1.0e-07	0.7689	718

Table 14: Efficiency comparison for several methods: A- the $\mu(x)$ method, B- the adjoint $\mu(x)$ method, C- the hybrid method, D- the method of Lee and Stewart (using an adaptive mesh in z), E- the method of Lee and Stewart using a 4th order fixed mesh Runge Kutta solver, F- the polar adjoint method, and G- the polar adjoint radial method. Here $\mathcal{E}=40$, q=0.3, $C=10^{21\mathcal{E}/40}$, and $\phi(u)=Ce^{-\mathcal{E}/T(u)}$, $T(u)=1-(u-1.5)^2$.

	$\lambda = 1$			$\lambda = i$			$\lambda = 10$			$\lambda = 10i$		
	Tol	Time	pnts	Tol	Time	Mesh	Tol	Time	Mesh	Tol	Time	Mesh
A	1.0e-08	0.14	159	1.0e-08	0.17	168	1.0e-07	0.22	250	1.0e-08	0.46	493
В	1.0e-08	0.19	221	1.0e-08	0.21	226	1.0e-08	0.37	445	1.0e-08	0.87	944
C	1.0e-08	0.15	176	1.0e-08	0.19	199	1.0e-07	0.23	273	1.0e-08	0.85	942
D	1.0e-08	0.22	273	1.0e-07	0.15	163	1.0e-08	0.63	793	1.0e-08	0.68	765
E	9.82e-07	12	32768	8.75e-07	13	32768	1.78e-07	23	65536	1.62e-07	26	65536
F	1.0e-03	0.026	23	1.0e-06	0.08	76	1.0e-03	0.054	57	1.0e-07	0.55	585
G	1.0e-08	0.2300	242	1.0e-07	0.1879	174	10e-08	0.4368	458	1.0e-07	0.6668	620

Table 15: Efficiency comparison for several methods: A- the $\mu(x)$ method, B- the adjoint $\mu(x)$ method, C- the hybrid method, D- the method of Lee and Stewart (using an adaptive mesh in z), E- the method of Lee and Stewart using a 4th order fixed mesh Runge Kutta solver, F- the polar adjoint method, and G- the polar adjoint radial method. Here $\mathcal{E}=40$, q=0.47, $C=10^{21\mathcal{E}/40}$, and $\phi(u)=Ce^{-\mathcal{E}/T(u)}$, $T(u)=1-(u-1.5)^2$.

	$\lambda = 1$			$\lambda = i$			$\lambda = 10$			$\lambda = 10i$		
	Tol	Time	pnts	Tol	Time	Mesh	Tol	Time	Mesh	Tol	Time	Mesh
A	1.0e-03	0.011	9	1.0e-03	0.011	8	1.0e-02	0.026	24	1.0e-03	0.037	33
В	1.0e-03	0.0082	6	1.0e-04	0.011	8	1.0e-02	0.021	21	1.0e-04	0.038	38
C	1.0e-03	0.011	9	1.0e-04	0.016	12	1.0e-02	0.026	26	1.0e-04	0.059	60
D	1.0e-04	0.029	29	1.0e-07	0.039	43	1.0e-08	0.34	423	1.0e-08	0.37	419
E	7.2e-07	0.046	128	8.2e-07	0.052	128	1.8e-07	1.5	4096	1.8e-07	1.6	4096
F	1.0e-03	0.0092	6	1.0e-05	0.011	9	1.0e-02	0.02	21	1.0e-04	0.039	38
G	1.0e-04	0.0183	18	1.0e-04	0.0206	18	1.0e-04	0.067	70			

Table 16: Efficiency comparison for several methods: A- the $\mu(x)$ method, B- the adjoint $\mu(x)$ method, C- the hybrid method, D- the method of Lee and Stewart (using an adaptive mesh in z), E- the method of Lee and Stewart using a 4th order fixed mesh Runge Kutta solver, F- the polar adjoint method, and G- the polar adjoint radial method. Here $\mathcal{E}=1$, q=0.1, $C=e^{\mathcal{E}/2}$, and $\phi(u)=Ce^{-\mathcal{E}/u}$.

	$\lambda = 1$			$\lambda = i$			$\lambda = 10$			$\lambda = 10i$		
	Tol	Time	pnts	Tol	Time	Mesh	Tol	Time	Mesh	Tol	Time	Mesh
A	1.0e-02	0.011	9	1.0e-03	0.013	10	1.0e-02	0.028	28	1.0e-03	0.044	44
В	1.0e-04	0.0099	10	1.0e-04	0.011	10	1.0e-02	0.024	26	1.0e-05	0.086	91
C	1.0e-02	0.012	10	1.0e-04	0.016	13	1.0e-02	0.027	30	1.0e-04	0.074	79
D	1.0e-06	0.036	44	1.0e-08	0.059	66	1.0e-08	0.43	532	1.0e-08	0.47	532
E	6.4e-07	0.092	256	7e-07	0.1	256	7.6e-08	2.9	8192	7.8e-08	3.3	8192
F	1.0e-04	0.012	11	1.0e-04	0.011	10	1.0e-04	0.028	32	1.0e-05	0.086	91
G	1.0e-04	0.0251	25	1.0e-04	0.0280	25	1.0e-05	0.1018	106	1.0e-05	0.1326	122

Table 17: Efficiency comparison for several methods: A- the $\mu(x)$ method, B- the adjoint $\mu(x)$ method, C- the hybrid method, D- the method of Lee and Stewart (using an adaptive mesh in z), E- the method of Lee and Stewart using a 4th order fixed mesh Runge Kutta solver, F- the polar adjoint method, and G- the polar adjoint radial method. Here $\mathcal{E}=1,\ q=0.3,\ C=e^{\mathcal{E}/2},$ and $\phi(u)=Ce^{-\mathcal{E}/u}.$

	$\lambda = 1$			$\lambda = i$			$\lambda = 10$			$\lambda = 10i$		
	Tol	Time	pnts	Tol	Time	Mesh	Tol	Time	Mesh	Tol	Time	Mesh
A	1.0e-03	0.014	14	1.0e-04	0.021	19	1.0e-02	0.035	38	1.0e-03	0.075	79
В	1.0e-05	0.02	23	1.0e-05	0.024	25	1.0e-03	0.034	40	1.0e-05	0.17	185
C	1.0e-03	0.016	16	1.0e-05	0.028	28	1.0e-02	0.034	40	1.0e-04	0.13	137
D	1.0e-07	0.063	76	1.0e-08	0.086	96	1.0e-08	0.67	840	1.0e-08	0.75	854
E	1.5e-07	0.37	1024	1.7e-07	0.41	1024	2.5e-07	5.9	16384	2.6e-07	6.5	16384
F	1.0e-05	0.02	23	1.0e-06	0.035	36	1.0e-04	0.044	52	1.0e-05	0.17	185
G	1.0e-05	0.0493	51	1.0e-06	0.0783	72	1.0e-06	0.2847	297	1.0e-05	0.3128	290

Table 18: Efficiency comparison for several methods: A- the $\mu(x)$ method, B- the adjoint $\mu(x)$ method, C- the hybrid method, D- the method of Lee and Stewart (using an adaptive mesh in z), E- the method of Lee and Stewart using a 4th order fixed mesh Runge Kutta solver, F- the polar adjoint method, and G- the polar adjoint radial method. Here $\mathcal{E}=1$, q=0.47, $C=e^{\mathcal{E}/2}$, and $\phi(u)=Ce^{-\mathcal{E}/u}$.

	$\lambda = 1$			$\lambda = i$			$\lambda = 10$			$\lambda = 10i$		
	Tol	Time	pnts	Tol	Time	Mesh	Tol	Time	Mesh	Tol	Time	Mesh
A	1.0e-02	0.01	8	1.0e-04	0.016	13	1.0e-02	0.027	27	1.0e-03	0.046	45
В	1.0e-03	0.0089	8	1.0e-04	0.012	10	1.0e-03	0.024	26	1.0e-04	0.052	55
C	1.0e-02	0.0096	8	1.0e-04	0.017	14	1.0e-02	0.027	29	1.0e-04	0.069	74
D	1.0e-06	0.038	46	1.0e-07	0.044	49	1.0e-08	0.4	497	1.0e-08	0.44	500
E	3.3e-07	0.092	256	3.3e-07	0.1	256	5.6e-07	1.5	4096	5.9e-07	1.6	4096
F	1.0e-03	0.0092	8	1.0e-04	0.012	10	1.0e-02	0.024	25	1.0e-04	0.053	55
G	10e-04	0.0202	20	1.0e-04	0.0240	21	1.0e-04	0.0811	84	1.0e-04	01229	113

Table 19: Efficiency comparison for several methods: A- the $\mu(x)$ method, B- the adjoint $\mu(x)$ method, C- the hybrid method, D- the method of Lee and Stewart (using an adaptive mesh in z), E- the method of Lee and Stewart using a 4th order fixed mesh Runge Kutta solver, F- the polar adjoint method, and G- the polar adjoint radial method. Here $\mathcal{E} = 10$, q = 0.1, $C = e^{\mathcal{E}/2}$, and $\phi(u) = Ce^{-\mathcal{E}/u}$.

	$\lambda = 1$			$\lambda = i$			$\lambda = 10$			$\lambda = 10i$		
	Tol	Time	pnts	Tol	Time	Mesh	Tol	Time	Mesh	Tol	Time	Mesh
A	1.0e-03	0.014	13	1.0e-05	0.035	32	1.0e-02	0.047	50	1.0e-04	0.14	155
В	1.0e-02	0.0082	8	1.0e-05	0.027	28	1.0e-03	0.043	49	1.0e-05	0.21	228
C	1.0e-02	0.013	12	1.0e-05	0.033	32	1.0e-02	0.045	52	1.0e-05	0.24	260
D	1.0e-07	0.076	93	1.0e-08	0.1	116	1.0e-08	0.81	1027	1.0e-08	0.9	1037
E	2.6e-07	0.37	1024	3e-07	0.41	1024	4.5e-07	5.8	16384	4.8e-07	6.6	16384
F	1.0e-04	0.013	14	1.0e-06	0.041	42	1.0e-05	0.062	71	1.0e-05	0.21	228
G	1.0e-03	0.031	32	1.0e-05	0.0528	48	1.0e-06	0.2576	269	1.0e-05	0.3669	339

Table 20: Efficiency comparison for several methods: A- the $\mu(x)$ method, B- the adjoint $\mu(x)$ method, C- the hybrid method, D- the method of Lee and Stewart (using an adaptive mesh in z), E- the method of Lee and Stewart using a 4th order fixed mesh Runge Kutta solver, F- the polar adjoint method, and G- the polar adjoint radial method. Here $\mathcal{E}=10$, q=0.3, $C=e^{\mathcal{E}/2}$, and $\phi(u)=Ce^{-\mathcal{E}/u}$.

	$\lambda = 1$			$\lambda = i$			$\lambda = 10$			$\lambda = 10i$		
	Tol	Time	pnts	Tol	Time	Mesh	Tol	Time	Mesh	Tol	Time	Mesh
A	1.0e-03	0.029	31	1.0e-08	0.5	540	1.0e-02	0.14	174	1.0e-09	7.3	8009
В	1.0e-02	0.019	22	1.0e-08	0.51	542	1.0e-04	0.16	186	1.0e-08	4.7	5160
C	1.0e-03	0.028	31	1.0e-08	0.5	542	1.0e-02	0.14	176	1.0e-08	4.7	5169
D	1.0e-08	0.38	482	1.0e-08	0.42	481	1.0e-09	5.9	7352	1.0e-09	6.6	7464
E	1.6e-07	5.9	16384	1.4e-07	6.6	16384						
F	1.0e-03	0.026	29	1.0e-06	0.19	201	1.0e-04	0.21	245	1.0e-06	1.8	1933
G	1.0e-07	0.3950	411	1.0e-06	0.6063	565	1.0e-07	3.1675	3218	1.0e-06	6.0556	5575

Table 21: Efficiency comparison for several methods: A- the $\mu(x)$ method, B- the adjoint $\mu(x)$ method, C- the hybrid method, D- the method of Lee and Stewart (using an adaptive mesh in z), E- the method of Lee and Stewart using a 4th order fixed mesh Runge Kutta solver, F- the polar adjoint method, and G- the polar adjoint radial method. Here $\mathcal{E}=10$, q=0.47, $C=e^{\mathcal{E}/2}$, and $\phi(u)=Ce^{-\mathcal{E}/u}$.

	$\lambda = 1$			$\lambda = i$			$\lambda = 10$			$\lambda = 10i$		
	Tol	Time	pnts	Tol	Time	Mesh	Tol	Time	Mesh	Tol	Time	Mesh
A	1.0e-02	0.011	9	1.0e-05	0.022	19	1.0e-02	0.032	33	1.0e-04	0.08	84
В	1.0e-02	0.0081	7	1.0e-05	0.016	16	1.0e-04	0.031	35	1.0e-05	0.11	113
C	1.0e-02	0.011	10	1.0e-05	0.021	20	1.0e-02	0.033	36	1.0e-05	0.14	148
D	1.0e-06	0.041	50	1.0e-07	0.048	54	1.0e-08	0.48	595	1.0e-08	0.53	597
E	8.1e-08	0.18	512	8e-08	0.21	512						
F	1.0e-03	0.0083	8	1.0e-03	0.0092	8	1.0e-02	0.027	30	1.0e-04	0.07	74
G	1.0e-04	0.0232	23	1 0e-04	0.0282	25	1.0e-05	0.1116	115	1.0e-05	0.1686	155

Table 22: Efficiency comparison for several methods: A- the $\mu(x)$ method, B- the adjoint $\mu(x)$ method, C- the hybrid method, D- the method of Lee and Stewart (using an adaptive mesh in z), E- the method of Lee and Stewart using a 4th order fixed mesh Runge Kutta solver, F- the polar adjoint method, and G- the polar adjoint radial method. Here $\mathcal{E}=20$, q=0.1, $C=e^{\mathcal{E}/2}$, and $\phi(u)=Ce^{-\mathcal{E}/u}$.

	$\lambda = 1$			$\lambda = i$			$\lambda = 10$			$\lambda = 10i$		
	Tol	Time	pnts	Tol	Time	Mesh	Tol	Time	Mesh	Tol	Time	Mesh
A	1.0e-03	0.021	22	1.0e-09	0.4	418	1.0e-02	0.093	106	1.0e-09	3.5	3852
В	1.0e-04	0.022	26	1.0e-09	0.41	424	1.0e-03	0.091	107	1.0e-08	2.3	2529
C	1.0e-04	0.026	30	1.0e-09	0.4	423	1.0e-02	0.09	108	1.0e-08	2.3	2532
D	1.0e-08	0.21	265	1.0e-08	0.22	246	1.0e-09	2.9	3668	1.0e-09	3.2	3705
E	1.8e-07	1.5	4096	1.6e-07	1.6	4096						
F	1.0e-03	0.017	19	1.0e-06	0.094	100	1.0e-04	0.11	128	1.0e-05	0.54	583
G	1.0e-05	0.0874	90	1.0e-06	0.1626	149	1.0e-06	0.7249	740	1.0e-06	1.3564	1255

Table 23: Efficiency comparison for several methods: A- the $\mu(x)$ method, B- the adjoint $\mu(x)$ method, C- the hybrid method, D- the method of Lee and Stewart (using an adaptive mesh in z), E- the method of Lee and Stewart using a 4th order fixed mesh Runge Kutta solver, F- the polar adjoint method, and G- the polar adjoint radial method. Here $\mathcal{E}=20,\ q=0.3,\ C=e^{\mathcal{E}/2},\ \mathrm{and}\ \phi(u)=Ce^{-\mathcal{E}/u}.$

	$\lambda = 1$			$\lambda = i$			$\lambda = 10$			$\lambda = 10i$		
	Tol	Time	pnts	Tol	Time	Mesh	Tol	Time	Mesh	Tol	Time	Mesh
A	1.0e-03	0.13	156	1.0e-09	7.8	8654	1.0e-02	1.2	1412	1.0e-10	1.3e+02	136649
В	1.0e-05	0.18	221	1.0e-09	8	8670	1.0e-04	1.2	1430	1.0e-10	1.3e+02	136946
С	1.0e-04	0.15	175	1.0e-09	7.9	8657	1.0e-03	1.2	1419	1.0e-10	1.3e+02	136948
D	-	-	-	1.0e-10	319.6	258949	-	-	-	1.0e-11	9270.4	3.9e06
E	5.9e-07	96	262144	5.2e-08	1.1e+02	262144						
F	1.0e-04	0.18	218	1.0e-07	2.7	2882	1.0e-03	2.1	2023	1.0e-07	27	28684
G	1.0e-07	5.8414	5911	1.0e-07	18.2622	16857	-	-	-	-	-	-

Table 24: Efficiency comparison for several methods: A- the $\mu(x)$ method, B- the adjoint $\mu(x)$ method, C- the hybrid method, D- the method of Lee and Stewart (using an adaptive mesh in z), E- the method of Lee and Stewart using a 4th order fixed mesh Runge Kutta solver, F- the polar adjoint method, and G- the polar adjoint radial method. Here $\mathcal{E} = 20$, q = 0.47, $C = e^{\mathcal{E}/2}$, and $\phi(u) = Ce^{-\mathcal{E}/u}$.

Acknowledgement. K.Z. thanks the University of Paris 13 for their hospitality during a visit in which this work was partly carried out. The numerical Evans function computations performed in this paper were carried out using the STABLAB package developed by Jeffrey Humpherys with help of the authors.

References

- [BHZ] B. Barker, J. Humpherys, and K. Zumbrun, One-dimensional stability of parallel shock layers in isentropic magnetohydrodynamics, to appear, J. Diff. Eq.
- [BLZ] B. Barker, O. Lafitte and K. Zumbrun, Existence and stability of viscous shock profiles for 2-D isentropic MHD with infinite electrical resistivity, Acta Math. Sci. Ser. B Engl. Ed. 30 (2010), no. 2, 447–498.
- [BLeZ] B. Barker, M. Lewicka and K. Zumbrun, Existence and stability of viscoelastic shock profiles, to appear, Arch. Ration. Mech. Anal.
- [BMR] A. Bourlioux, A. Majda, and V. Roytburd, Theoretical and numerical structure for unstable one-dimensional detonations. SIAM J. Appl. Math. 51 (1991) 303–343.
- [Br] L. Q. Brin, Numerical testing of the stability of viscous shock waves. Math. Comp. 70 (2001) 235, 1071–1088.
- [BrZ] L. Brin and K. Zumbrun, Analytically varying eigenvectors and the stability of viscous shock waves. Seventh Workshop on Partial Differential Equations, Part I (Rio de Janeiro, 2001). Mat. Contemp. 22 (2002), 19–32.
- [CJLW] N. Costanzino, K. Jenssen, G. Lyng, and M. Williams, Existence and stability of curved multidimensional detonation fronts, Indiana Univ. Math. J. 56 (2007), no. 3, 1405–1461.
- [Er1] J. J. Erpenbeck, Stability of steady-state equilibrium detonations, Phys. Fluids 5 (1962), 604–614.
- [Er2] J. J. Erpenbeck, Stability of idealized one-reaction detonations, Phys. Fluids 7 (1964).
- [FD] W. Fickett and W.C. Davis, *Detonation*, University of California Press, Berkeley, CA (1979): reissued as *Detonation: Theory and experiment*, Dover Press, Mineola, New York (2000), ISBN 0-486-41456-6.
- [GZ] R. Gardner and K. Zumbrun, The Gap Lemma and geometric criteria for instability of viscous shock profiles. Comm. Pure Appl. Math. 51 (1998), no. 7, 797–855.

- [HLZ] J. Humpherys, O. Lafitte, and K. Zumbrun, Stability of viscous shock profiles in the high Mach number limit, to appear, Comm. Math. Phys.
- [HLyZ] J. Humpherys, G. Lyng, and K. Zumbrun, Spectral stability of ideal gas shock layers, to appear, Arch. for Rat. Mech. Anal.
- [HuZ1] J. Humpherys and K. Zumbrun, Numerical stability analysis of detonation waves in ZND, preprint (2010).
- [HuZ2] J. Humpherys and K. Zumbrun, An efficient shooting algorithm for Evans function calculations in large systems, Phys. D 220 (2006), no. 2, 116–126.
- [JLW] H.K. Jenssen, G. Lyng, and M. Williams. Equivalence of low-frequency stability conditions for multidimensional detonations in three models of combustion, Indiana Univ. Math. J. 54 (2005) 1–64.
- [JY] S. Jung and J. Yao, Stability of ZND detonations for Majda's model, to appear, Quarterly Appl. Math.
- [LS] H. I. Lee and D. S. Stewart. Calculation of linear detonation instability: one-dimensional instability of plane detonation, J. Fluid Mech., 216 (1990), 103–132, 1990.
- [LyZ1] G. Lyng and K. Zumbrun, One-dimensional stability of viscous strong detonation waves, Arch. Ration. Mech. Anal. 173 (2004), no. 2, 213–277.
- [LyZ2] G. Lyng and K. Zumbrun, A stability index for detonation waves in Majda's model for reacting flow, Physica D, 194 (2004), 1–29.
- [M1] A. Majda, A qualitative model for dynamic combustion, SIAM J. Appl. Math., 41 (1981), 70–91.
- [M2] A. Majda, Compressible fluid flow and systems of conservation laws in several space variables. Springer-Verlag, New York (1984), viii+ 159 pp.
- [MaZ3] C. Mascia and K. Zumbrun, Pointwise Green function bounds for shock profiles of systems with real viscosity. Arch. Ration. Mech. Anal. 169 (2003), no. 3, 177–263.
- [MeZ1] G. Métivier and K. Zumbrun, Large viscous boundary layers for noncharacteristic nonlinear hyperbolic problems, Mem. Amer. Math. Soc. 175 (2005), no. 826, vi+107 pp.
- [PZ] Plaza, R. and Zumbrun, K., An Evans function approach to spectral stability of small-amplitude shock profiles, J. Disc. and Cont. Dyn. Sys. 10. (2004), 885-924.
- [Z1] K. Zumbrun, Stability of detonation waves in the ZND limit, to appear, Arch. Ration. Mech. Anal.
- [Z2] K. Zumbrun. A local greedy algorithm and higher order extensions for global numerical continuation of analytically varying subspaces, to appear, Quart. Appl. Math.
- [Z3] K. Zumbrun. Numerical error analysis for evans function computations: a numerical gap lemma, centered-coordinate methods, and the unreasonable effectiveness of continuous orthogonalization, Preprint (2009).
- [Z4] K. Zumbrun, High-frequency asymptotics and stability of ZND detonations in the high-overdrive and small-heat release limits, Preprint (2010).
- [Z5] K. Zumbrun, Stability of noncharacteristic boundary layers in the standing-shock limit, to appear, Trans. Amer. Math. Soc.